

AD-A098 164

HUGHES AIRCRAFT CO CULVER CITY CA LASER SYSTEMS DIV

F/6 20/5

PULSED RF WAVEGUIDE STUDIES PROGRAM.(U)

MAY 80 L V SUTTER

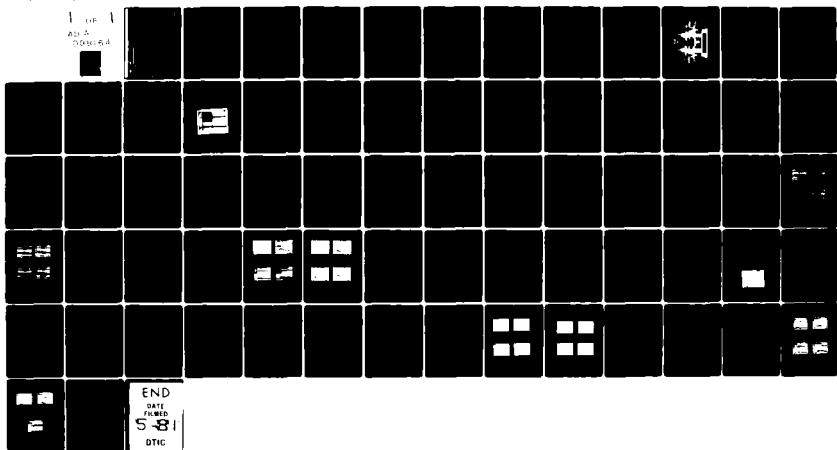
DAA807-78-C-2450

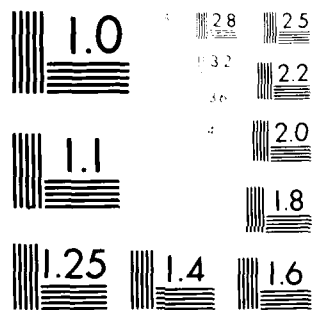
UNCLASSIFIED

HAC-FR-80-72-997

DELVN-TR-78-2450-1-2

NL

UP  
AD-A  
0000-64



MILITARY ACADEMY, 1915, N. Y. 10003  
 U. S. ARMY, 1915, N. Y. 10003

**LEVEL III**

**(12)**

B.S.

RESEARCH AND DEVELOPMENT TECHNICAL REPORT  
DELNV-TR-78-200-1 ✓

AD A 098164

## **PULSED RF WAVEGUIDE STUDIES PROGRAM**

L. V. Sutter  
Hughes Aircraft Company  
Centinela & Teale Streets  
Culver City, CA

May 1980

**DTIC**  
**ELECTE**  
APR 23 1981  
**S D E**

Final Report for Period July 1978 to April 1980

Distribution Statement  
Approved to public release  
distribution unlimited.

Prepared for:  
**NIGHT VISION & ELECTRO OPTICS LABORATORY**  
Fort Belvoir, Virginia

**ERADCOM**

US ARMY ELECTRONICS RESEARCH AND DEVELOPMENT COMMAND  
FORT BELVOIR, VIRGINIA

Report No. PR-80-72-007  
MAY 78 100-10

**R 1 4 23 018**

HAC Report No. FR-80-72-997 ✓

PULSED RF WAVEGUIDE STUDIES PROGRAM.

9 FINAL REPORT. Jul 78-1-1-80

Prepared for  
NVEOL  
Fort Belvoir, Virginia

Prepared by  
11 L. V./Sutter  
Program Manager

15  
Contract No. DAAB07-78-C-2450  
July 1978 through August 1980

11 May 1980

18 DEL NV  
19 TR-78-2450-1-2

Laser Systems Division  
Electro-Optical and Data Systems Group  
Hughes Aircraft Company • Culver City, California

4150-50-1

## TABLE OF CONTENTS

INTRODUCTION .....	1
DEVICE DESCRIPTION .....	3
POWER ELECTRONICS DESCRIPTION .....	6
LASER HEAD ELECTRONICS MODEL .....	9
Determination of $C$ , $\bar{C}$ , and $L$ .....	12
Determination of $R_1$ .....	13
Determination of $R_g$ .....	14
Determination of $N_e$ .....	17
Electrical Summary .....	17
LASER CHARACTERISTICS MODEL .....	18
Laser Kinetics Model .....	18
Power Output Efficiency .....	21
Gain-Switched Pulse Delay Time, $\tau_{gs}$ .....	26
SEALED LASER EXPERIMENTAL RESULTS .....	29
Sealed Gain Data .....	29
Experimental Setup and Discussion .....	29
Results .....	30
Sealed Power Output Data .....	36
Experimental Setup and Discussion .....	36
Results .....	37
Sealed Life Test Data .....	46
Results .....	46
Amplitude and Frequency Stability Data .....	47
Conclusions and Observations .....	49
ACKNOWLEDGEMENTS .....	50
REFERENCES .....	51
APPENDIX .....	A-1

# LIST OF ILLUSTRATIONS

Figure		Page
1	Pulsed RF Waveguide Laser .....	4
2	Laser Cross-Section Used in the Experiments .....	5
3	Power Electronics Layout .....	7
4	Typical RF Matching Network with Approximate Range of Values of the Circuit Elements .....	8
5	Laser Head Lumped Circuit Model .....	9
6	Typical Forward and Reflected Voltage Waveforms .....	10
7	Theoretical Vs Experimental Impedance for Laser Head, No Discharge .....	13
8	Electron Drift Velocity Vs E/N for Various Gas Mixes .....	16
9	The Characteristic Decay Time, $\tau_i$ , for Various Collision Partners .....	22
10	Small Signal Gain Experimental Apparatus .....	30
11	$g_p$ Versus $\tau_p$ for Various Gas Mixes at $P = 125$ Torr, $P_{lh} = 2.0$ kW, and $f_p = 1.0$ kHz .....	33
12	Typical Small Signal Gain Data for 3:1:1 and 8:1:1 Mixes with $X_e$ .....	34
13	Typical Small Signal Gain Data for (3:0:1) Plus $H_2O$ and $X_e$ With and Without $N_2$ .....	35
14	Sealed Power Output Experimental Apparatus .....	36
15	Typical Laser Power Output Data for 3:1:1 and 8:1:1 Mixes with $X_e$ .....	39
16	Typical Laser Power Output Data for (3:0:1) Plus $H_2O$ and $X_e$ With and Without $N_2$ .....	40
17	$P_{ave}$ Versus $\tau_p$ for Various Gas Mixes at $P = 125$ Torr, $f_p = 1.0$ kHz, and $P_{lh} = 2.0$ kW .....	41
18	$P_{ave}$ Versus $X_e$ Content for (3:0:1) + 1.0% $H_2O$ Mix at $P = 125$ Torr, $\tau_p = 3.0$ $\mu$ sec, and $P_{lh} = 2.0$ kW .....	42

# LIST OF ILLUSTRATIONS (CONTINUED)

Figure		Page
19	$P_p$ Versus $f_p$ for 86.3% (3:0:1) + 12.8% $X_e$ + 0.9% $H_2O$ Mix at $P = 125$ Torr, $\tau_p = 3.0 \mu\text{sec}$ , and $P_{\ell h} = 2.0 \text{ kW}$ . . . .	43
20	$E_p$ Versus $f_p$ for 86.3% (3:0:1) + 12.8% $X_e$ + 0.9% $H_2O$ at $P = 125$ Torr, $\tau_p = 3.0 \mu\text{sec}$ and $P_{\ell h} = 2.0 \text{ kW}$ . . . . .	44
21	$\eta_l$ Versus $\tau_p$ for Various Gas Mixes at $P = 125$ Torr, $f_p = 1.0 \text{ kHz}$ , and $P_{\ell h} = 2.0 \text{ kW}$ . . . . .	45
22	Typical Multipulse Laser Output with $P_{\ell h} = 2.0 \text{ kW}$ , $f_p = 1.0 \text{ kHz}$ , and $\tau_p = 3.0 \mu\text{sec}$ . . . . .	47
23	Typical Single Pulse Heterodyne Signal of the Pulsed rf Laser, and a cw Reference with $P_{\ell h} \approx 2.0 \text{ kW}$ , $f_p = 2.0 \text{ kHz}$ , and $\tau_p = 3.0 \mu\text{sec}$ . . . . .	48
A1	Gas Plumbing Layout for Flowing Gas Experiments . . . . .	A-2
A2	Flowing Gas Small Signal Gain Experimental Apparatus . . . . .	A-3
A3	Typical Small Signal Gain Data with Flowing Gas for 3:1:1 and 8:1:1 Mixes at 100 Torr Gas Pressure . . . . .	A-6
A4	Typical Small Signal Gain Data with Flowing Gas for 3:0:1 Mix . . . . .	A-7
A5	Flowing Gas Power Output Experimental Apparatus . . . . .	A-9
A6	Typical Laser Output Data with Flowing Gas for 3:1:1 and 8:1:1 Gas Mixes at 100 Torr Gas Pressure . . . . .	A-11
A7	Typical Laser Output Data with Flowing Gas for 3:0:1 Mix . . . . .	A-12

## LIST OF TABLES

Table		Page
1	Sealed Small Signal Gain Data . . . . .	32
2	Sealed Power Output Data . . . . .	38
A1	Flowing Gas Small Signal Gain Data . . . . .	A-5
A2	Flowing Gas Power Output Data . . . . .	A-10

## INTRODUCTION

The purpose of the Pulsed RF Waveguide Studies Program was to demonstrate the feasibility of and perform parametric studies on flowing and sealed rf pumped CO<sub>2</sub> waveguide lasers. Hughes is pleased to report the successful completion of the Phase 1 and Phase 2 efforts.

This report will deal with both the theoretical and experimental aspects of the program including analysis of the data and an outline of the experimental equipment and procedures used to obtain the data. Detailed derivations of the equations used in the analysis will not be included but appropriate references will be noted whenever possible to aid the reader in locating supporting background material. Descriptions of the device contained within this report will be sufficient for a basic understanding of the physics without compromising certain proprietary engineering design information obtained on internal funding.

During Phase 1 of the program, flowing gas parametric performance studies were performed. This research has been published in the Phase 1 Report, DELNV-TR-78-2450-1.<sup>1</sup> The Phase 2 work covered aspects of sealed laser operation including parametric gain and power output results with life tests data. Two laser heads and one power supply were also built and delivered to NVEOL in this phase.

This report will primarily deal with Phase 2 results. The Phase 1 data is included as an Appendix to this report. Although the Phase 1 work involved flowing gas experiments and the Phase 2 work involved sealed experiments, comparison of the data sets is not directly available as many changes in internal laser construction, optimum laser gas mixes, and experimental arrangements occurred after Phase 1 and during Phase 2.

It should also be noted that the commercial pulsed rf power supply purchased for the Phase 1 effort did not perform to specification nor was the reliability of the internal electronics acceptable. At the time of the final data taking the supply output power performance was degrading rapidly such that no more than 1.6 kW average pulse power could be obtained at the end of the experiments. The supply was specified for 2.5 kW originally. Thus most of the data was taken at low output which were not optimum in terms of laser performance. Power loading tests performed early in Phase 1 while the power supply was still operating properly indicated that average pulse power loadings to 3.0 kW was not a problem although no laser performance data was taken during this time.

Prior to Phase 2, the power supply was refurbished and again power loadings in excess of 2.5 kW were obtained and no problems with the supply occurred during Phase 2.

The data obtained during this study was excellent and many notable accomplishments were realized. These results are sufficiently promising as to assure the pulsed rf laser a place in many tactical CO<sub>2</sub> systems.

## DEVICE DESCRIPTION

The laser used for these experiments was a transversely excited rf pumped CO<sub>2</sub> waveguide employing internal aluminum electrodes and ceramic walls. Both flowing gas and sealed off experiments were performed. Figure 1 is a view of the laser head fully assembled including part of the matching network.

The entire laser outer shell and the electrodes were composed of aluminum. AR coated ZnSe windows were attached to each end cap in order to perform gain measurements. AN fittings were used to attach the gas lines and external valves to the laser head for the flowing gas experiments.

The active pumped length of the laser was 19 cm. For the flowing gas experiments a 2.0 mm square bore with BeO side walls was used whereas in the sealed off experiments a 2.5 mm square bore with alumina side walls was used. Figure 2 illustrates the laser bore construction. The AR windows (less than 1 percent loss each) were located 2.5 mm from the end bore opening. The ZnSe windows were 2.0 mm thick. The reflectivity of the output coupling mirror was variable by interchanging optical elements. The other reflector of the resonator was 99.5 percent reflecting at 10.6 microns. The resonator was a flat-flat design. The laser head and all other peripheral optics were mounted on a rigid optical rail which itself was solidly mounted to a rigid optical table.

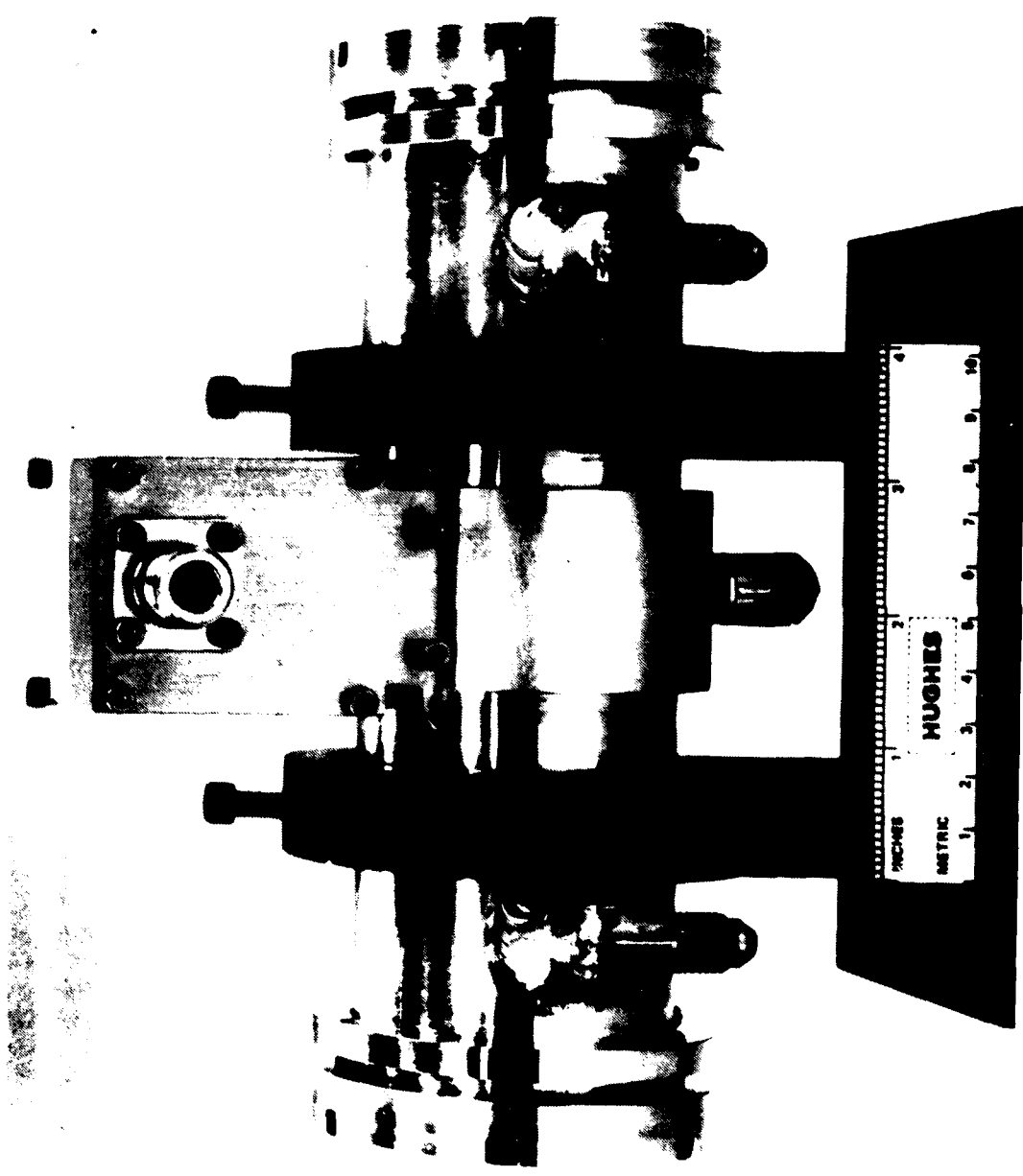


Figure 1. Pulsed RF waveguide laser.

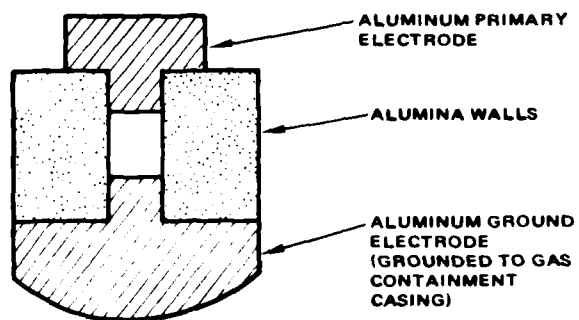


Figure 2. Laser cross-section used in the experiments.

## POWER ELECTRONICS DESCRIPTION

Figure 3 illustrates the electronics arrangement used during the sealed gas experiments for loading and measuring the power delivered to and reflected from the laser head.

A 50 ohm output impedance power supply was used as the rf source. The power was delivered to the matching network through a bi-directional coupler. Two attenuated ports (-23.6 dB) from the coupler allowed for low power measurement of the forward and reflected powers. These two ports were connected to an rf switch by which either port could be connected to a second attenuator (-40 dB) and thus observed on an oscilloscope. Thus the forward and reflected power pulses were monitored while simultaneously using the second trace of a dual trace scope to monitor signals from the infrared detector during gain and power output measurements. The reflected power returning towards the generator from the laser was dumped into a 50 ohm load by the use of a tuned 150 MHz circulator thus protecting the power supply during mismatched conditions. The forward power was matched into the laser head by a set of tuneable and fixed reactive elements located in the matching network and laser head.

The pulsed power supply used as the 50 ohm source was a modified EPSCO model No. 5231HB1 variable in power output (0 to 2.5 kW average power during the pulse), pulse width (0.3 to 10  $\mu$ sec), and repetition rate (0.1 to 20 kHz). The power output of the supply degraded during Phase 1 such that at the end of the primary experiments the best power obtainable from the supply was 1.6 kW, but prior to the Phase 2 experiments the supply was reconditioned to full power.

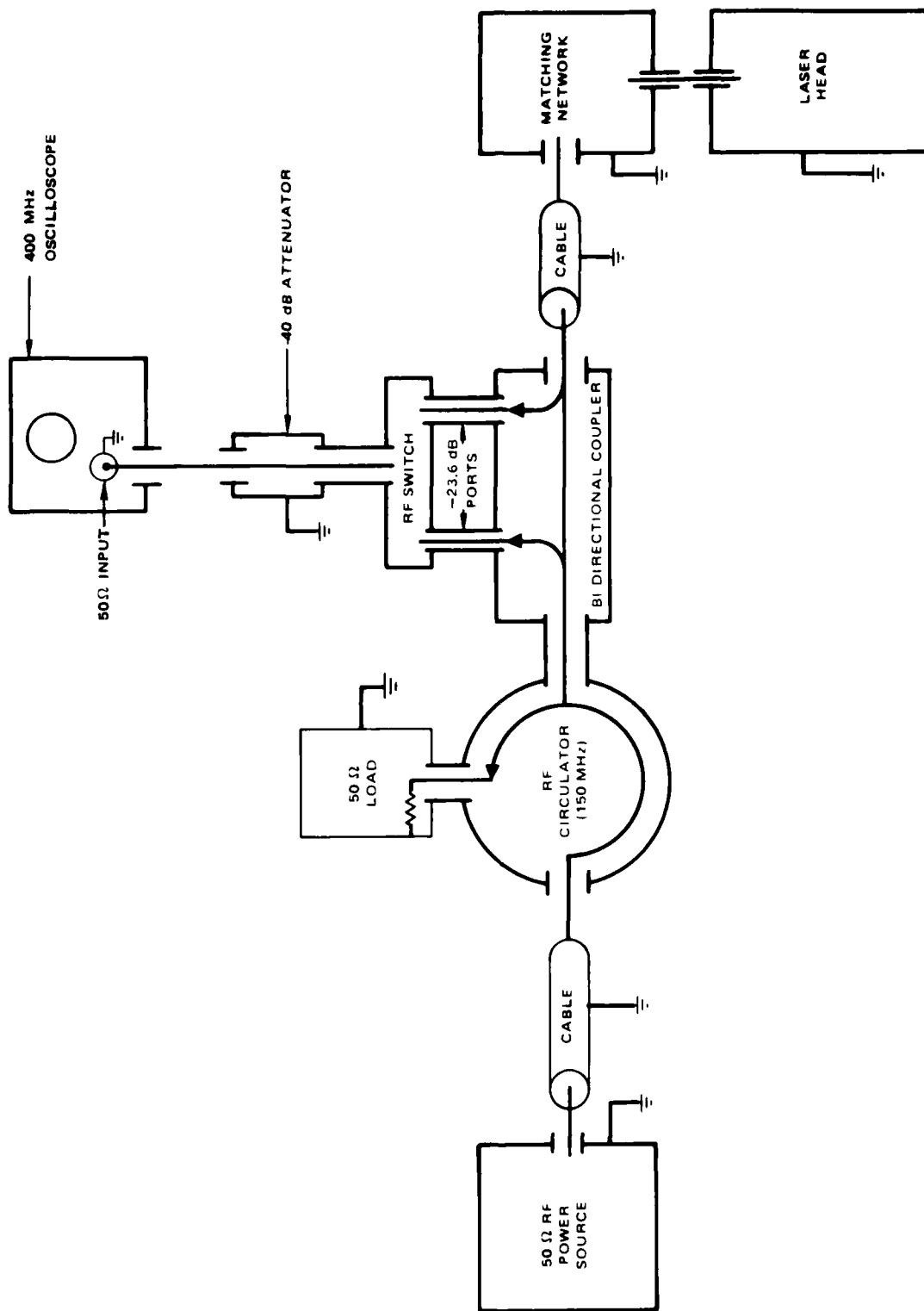


Figure 3. Power electronics layout.

The tuneable reactive elements in the matching network were piston-type capacitors. The pistons were driven by micrometers to improve the tuning accuracy of the capacitors. Figure 4 illustrates the rf matching network.

The interconnections between the independent circuit elements was obtained with RG213 cable and N-type connectors (50 ohms). This relatively large cable diameter was chosen to minimize power losses within the cable primarily due to the skin resistance of the center conductor, but the smaller standard RG58 cable would have also sufficed.

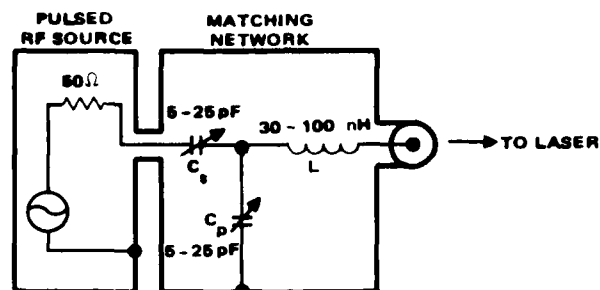
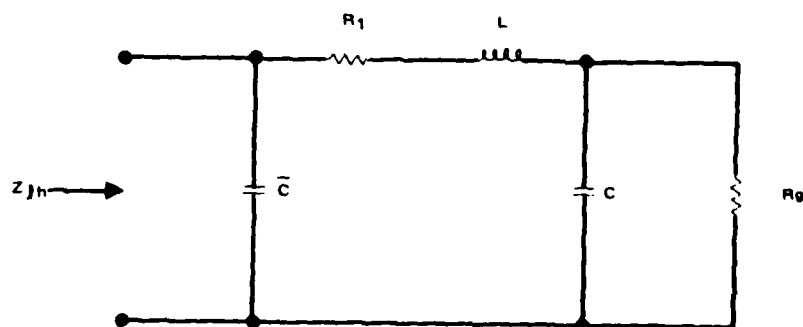


Figure 4. Typical rf matching network with approximate range of values of the circuit elements.

## LASER HEAD ELECTRONICS MODEL

Figure 5 illustrates the lumped equivalent circuit model of the laser head.  $R_g$  represents the effective resistance of the gas during the discharge. In reality  $R_g$  is not a constant and during the power pulse it will change in value such that the reflected power from the laser head will vary during the pulse. Prior to the power pulse the value of  $R_g$  can be considered nearly infinite at low pulse repetition rates (less than 20 kHz) since the residual plasma density of the previous pulse is rapidly quenched leaving a low conductivity condition. It was felt prior to Phase 1 that efficient passive matching of the power supply to the laser head in a pulsed mode would be difficult due to this temporal variation of  $R_g$ . In fact, this problem did not occur since the gas breakdown time was very rapid (less than 250 nsec) and after this breakdown time the gas resistance remained essentially constant for the rest of the pulse.

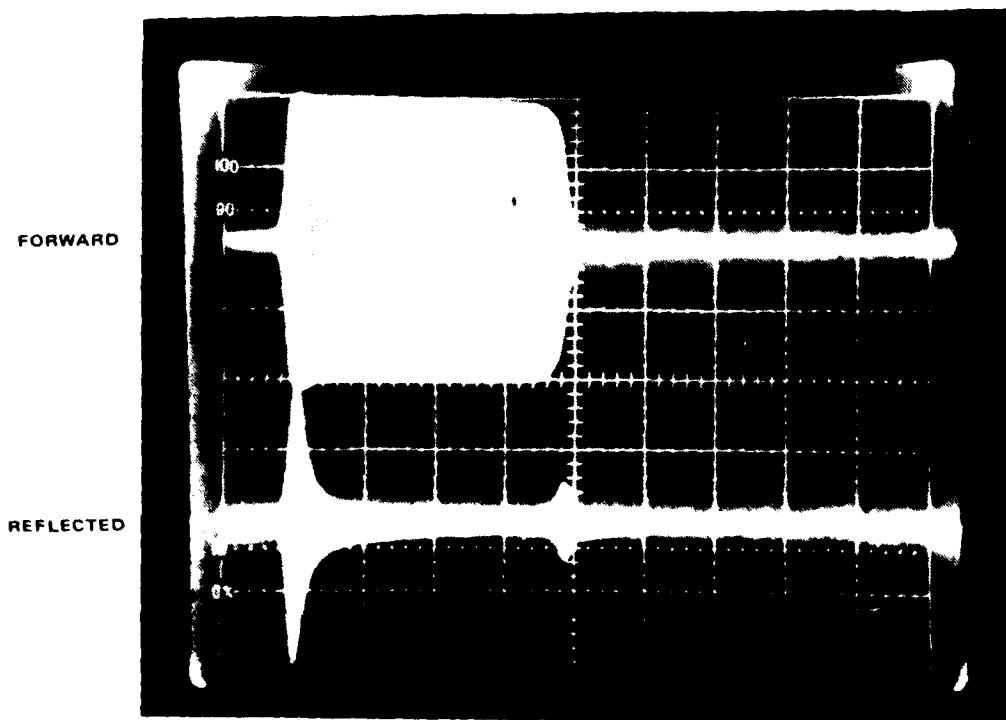


### NOMINAL CIRCUIT VALUES FOR PULSED RF LASER

- $\bar{C} \Rightarrow$  STRAY INPUT CAPACITANCE,  $\sim 2.4$  pF
- $R_1 \Rightarrow$  INPUT LEAD RESISTANCE,  $\sim 0.25 \Omega$
- $L \Rightarrow$  INPUT LEAD INDUCTANCE,  $\sim 82$  nH
- $C \Rightarrow$  DISCHARGE ELECTRODE CAPACITANCE,  $\sim 44$  pF
- $R_g \Rightarrow$  DISCHARGE RESISTANCE, 100 TO 500  $\Omega$  TYPICAL

Figure 5. Laser head lumped circuit model.

Figure 6 illustrates the actual forward and reflected rf envelope of the power pulse for a typical pulsed rf laser discharge. Note that the reflected power spike at the start of the pulse rapidly decays to a relatively low value for the duration of the pulse. Typically the reflected power after the initial spike can be held to less than 5 percent of the forward power even at powers of up to 3.0 kW. It is assumed that further increases in the power would maintain this low ratio of reflected to forward power up to the limit that gas overheating and subsequent rf arcing in the discharge occurred. The initial reflected power breakdown spike time appears to have some dependence with pulse power and generally the higher pulse powers require slightly less time for the gas to breakdown although this effect is not great.



DATA TAKEN WITH 43.6 dB ATTENUATION  
1.5 VOLT DIVISION  
1.0  $\mu$ SEC DIVISION

Figure 6. Typical forward and reflected voltage waveforms.

The lumped elements in the circuit of Figure 5 were determined in the following manner. With the laser head disconnected from the matching network, a Hewlett-Packard Vector Voltmeter coupled with a low power tunable rf source and bi-directional coupler was connected to the laser head. Without delving into the experimental aspects of this equipment, it will suffice to say that this equipment is capable of measuring the complex reflection coefficient,  $\rho$ , of the laser head versus rf frequency (see Reference 2 for background). The complex reflection coefficient is defined as the ratio of the complex values of the reflected divided by the forward electric field vectors. The value of  $\rho$  will in general be a function of frequency which allows for the determination of the effective lumped elements of the circuit model assuming the dimensions of the laser head are much smaller than the rf wavelength. For cases where the rf wavelength is an appreciable fraction of the discharge length, standing wave effects will occur such that the validity of the lumped model begins to fail. The wavelength of the rf within the discharge region will also decrease by  $\sqrt{\epsilon_r}$  (where  $\epsilon_r$  is the relative permittivity of the ceramic waveguide walls) whenever the parallel discharge capacitance,  $C$ , is dominated by the ceramic walls. The lumped circuit approach to the discharge model is valid for the laser used in these experiments.

The data obtained by the vector voltmeter for  $\rho$  is in the form of polar coordinates such that  $\rho$  is expressed as a magnitude  $|\rho|$  and angle  $\theta$ . This data can be converted into a complex impedance,  $Z = R + jX$ , either graphically by the use of a Smith Chart or algebraically by the relations:

$$R = Z_o \left( \frac{1 - |\rho|^2}{1 + |\rho|^2 - 2|\rho| \cos(\theta)} \right) \quad (1)$$

$$X = Z_o \left( \frac{2|\rho| \sin(\theta)}{1 + |\rho|^2 - 2|\rho| \cos(\theta)} \right) \quad (2)$$

where  $Z_o$  is the source impedance = 50 ohms.

Optimum matching of the rf power source to the laser head occurs when the impedance of the source as seen looking back through the matching network from the laser head is equal to the complex conjugate of the laser head impedance,  $Z_{lh}^*$ . Thus the purpose of the matching network is to transform the 50 ohms source impedance into the complex impedance  $Z_{lh}^*$  as seen by the laser head. For the lumped circuit model of Figure 5 and making the a priori assumption that this model is an accurate representation of the rf laser head impedance,  $Z_{lh}$ , can be expressed in terms of the separate circuit elements through the equation:

$$Z_{lh} = \frac{(ac + bd) + j(da - cb)}{a^2 + b^2} \quad (3)$$

where

$$\begin{aligned} a &= 1 - \omega^2 LC - \omega^2 C \bar{C} R_g R_1 \\ b &= \omega \bar{C} (R_g + R_1) - \omega^3 LC \bar{C} R_g + \omega C R_g \\ c &= R_1 + R_g - \omega^2 L C R_g \\ d &= \omega L + \omega C R_1 R_g \\ \omega &= 2\pi f \end{aligned}$$

#### DETERMINATION OF C, $\bar{C}$ , AND L

By taking values of  $\rho$  for the no discharge condition ( $R_g = \infty$ ) and assuming the capacitance across the discharge region, C, does not change appreciably between the discharge and no discharge conditions, and also assuming the laser head input lead resistance,  $R_1$ , is small, then the lumped values of C, the input lead inductance, L, and the stray input capacitance,  $\bar{C}$ , can be determined through the relation:

$$\frac{Z_0 \sin(\theta)}{1 - \cos(\theta)} = \frac{1 - \omega^2 LC}{\omega^3 L \bar{C} C - \omega(C + \bar{C})} \quad (4)$$

where the left side of the equation is from Equation (2) for  $|\rho| = 1$ . Thus by taking at least three values of  $\rho$  at three frequencies the laser head reactive lumped circuit elements can be determined. Figure 7 illustrates the match of the theoretical lumped circuit model impedance to the experimental impedance versus frequency of the laser head used in the flowing gas experiments.

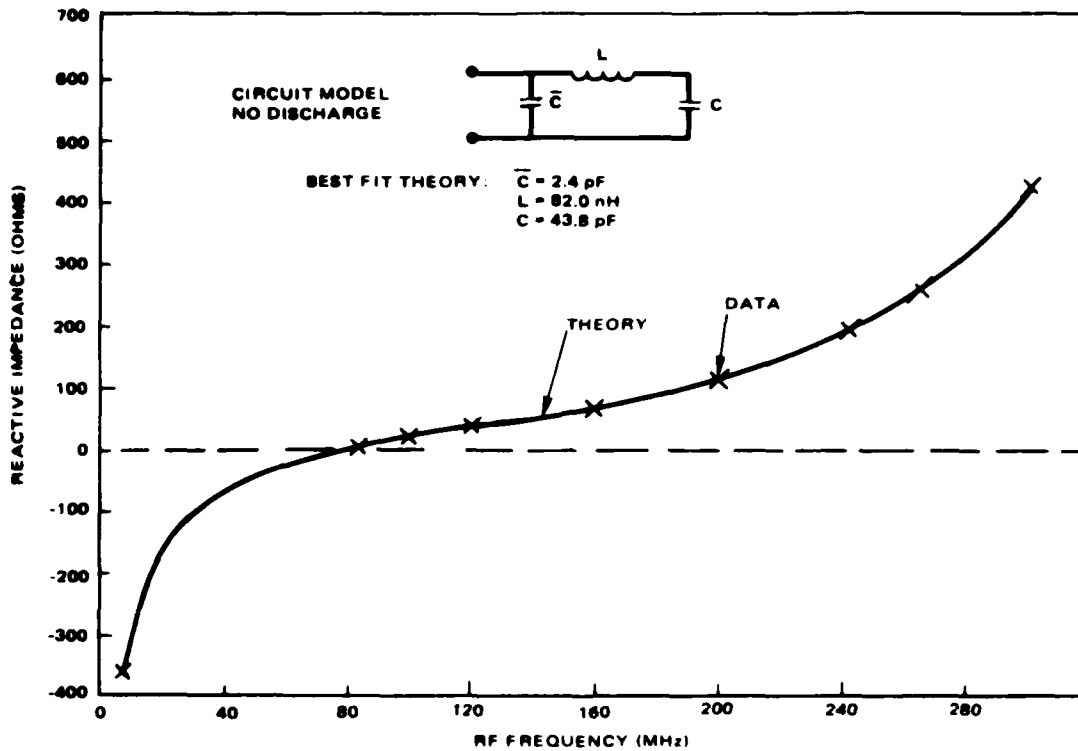


Figure 7. Theoretical vs experimental impedance for laser head, no discharge.

#### DETERMINATION OF $R_1$

The input lead resistance,  $R_1$ , is a source of unwanted power losses. Even small values of  $R_1$  can lead to significantly lowered power efficiency,  $\eta_d$ , where  $\eta_d$  is defined as the ratio of the power delivered to the gas discharge divided by the total power delivered to the laser head and is given by the equation:<sup>2</sup>

$$\eta_d = \frac{1}{1 + \frac{R_1(1 + \omega^2 C^2 R_g^2)}{R_g}} \quad (5)$$

For cases where  $C$  is large, even small values of  $R_1$  can lead to appreciable losses. For example consider a typical cw rf waveguide laser with  $R_g = 500$  ohms,  $C = 45$  pF, and  $f = \omega/2\pi = 150$  MHz and assume  $R_1 = 0.5$  ohms. For this case  $\eta_d = 0.69$  which is relatively poor especially considering that Hughes has built rf sources which convert 28 volt dc to rf with a conversion efficiency of nearly 85 percent. Typical values of  $R_1$  for properly designed rf lasers would be less than 0.5 ohm. Using the preceding data with  $R_1 = 0.1$  ohm yields  $\eta_d = 92$  percent. Lowering the value of  $C$  through low capacitance design will further increase the efficiency.

$R_1$  can be determined in the following manner. At the resonance point of the laser head without the discharge, the  $Q$  of the laser head will be:

$$Q = \frac{\bar{\omega}L}{R} = \frac{\bar{\omega}}{\Delta\omega} \quad (6)$$

where

$$\frac{1}{Q} = \left( \frac{1}{LC} \right)^{1/2}$$

and where the bandwidth of the resonant circuit,  $\Delta\omega$ , is measured as the full width at the 3 dB points. For the pulsed laser used in the flowing gas experiments,  $Q = 151$  at  $\bar{\omega} = 4.6 \times 10^8$  rad/sec and  $L = 82$  nH so that  $R_1 = 0.25$  ohm. In general the resonance point of the laser head is not the actual operating frequency of the power source such that the value of  $R_1$  obtained at resonance will differ slightly at the operating frequency due to the skin resistance effect which increases as the square root of frequency.

#### DETERMINATION OF $R_g$

The effective resistance of the gas discharge will vary with gas mix, bore size, power input, gas pressure, and rf frequency. The value of  $R_g$  for a given set of discharge parameters can be determined in the following manner. Once the reactive elements in the matching network have matched the laser head to the rf source, the impedance as seen from the laser head looking back at the source must be equal to the complex conjugate of the laser

head impedance,  $Z_{lh}$ . For measurement purposes it is desirable for the rf source to appear as an impedance,  $Z_o$ , where typically  $Z_o = 50$  ohms. It is important to note that in reality the rf source will not appear to be 50 ohms unless an rf circulator with a 50Ω reflected power port is used since the rf source impedance during the discharge is not known. If  $Z_{lh} = R_{lh} + iX_{lh}$  then from Equations (1), (2) and (3) it becomes obvious that the exact value of  $R_g$  can be determined by use of the equations:

$$R_{lh} = Z_o \left( \frac{1 - |\rho|^2}{1 + |\rho|^2 - 2|\rho|\cos(\theta)} \right) = \frac{ac + bd}{a^2 + b^2} \quad (7)$$

$$X_{lh} = Z_o \left( \frac{2|\rho|\sin(\theta)}{1 + |\rho|^2 - 2|\rho|\cos(\theta)} \right) = \frac{da - cb}{a^2 + b^2} \quad (8)$$

and thus by iterating Equations 7 and 8 on  $R_g$ , using the previously determined values of  $R_1$ ,  $C$ ,  $\bar{C}$ , and  $L$ , the value of  $R_g$  can be determined. For the pulsed rf laser used in the flowing gas experiments for a pulsed rf discharge in an 8:1:1 mix of He:N<sub>2</sub>:CO<sub>2</sub> at 100 Torr with an average pulse power of 2.0 kW,  $R_g$  was determined experimentally to be approximately 165Ω. The rms voltage across the discharge can then be calculated using the relation:

$$\eta_d P_{lh} = V_{rms}^2 / R_g \quad (9)$$

where  $P_{lh}$  is the average pulse power delivered to the laser head,  $V_{rms}$  is the rms pulse voltage across the discharge, and  $\eta_d$  is defined by Equation (5). Using the circuit elements of Figure 8 at 150 MHz,  $V_{rms} = 555$  volts assuming  $\eta_d = 0.93$ .

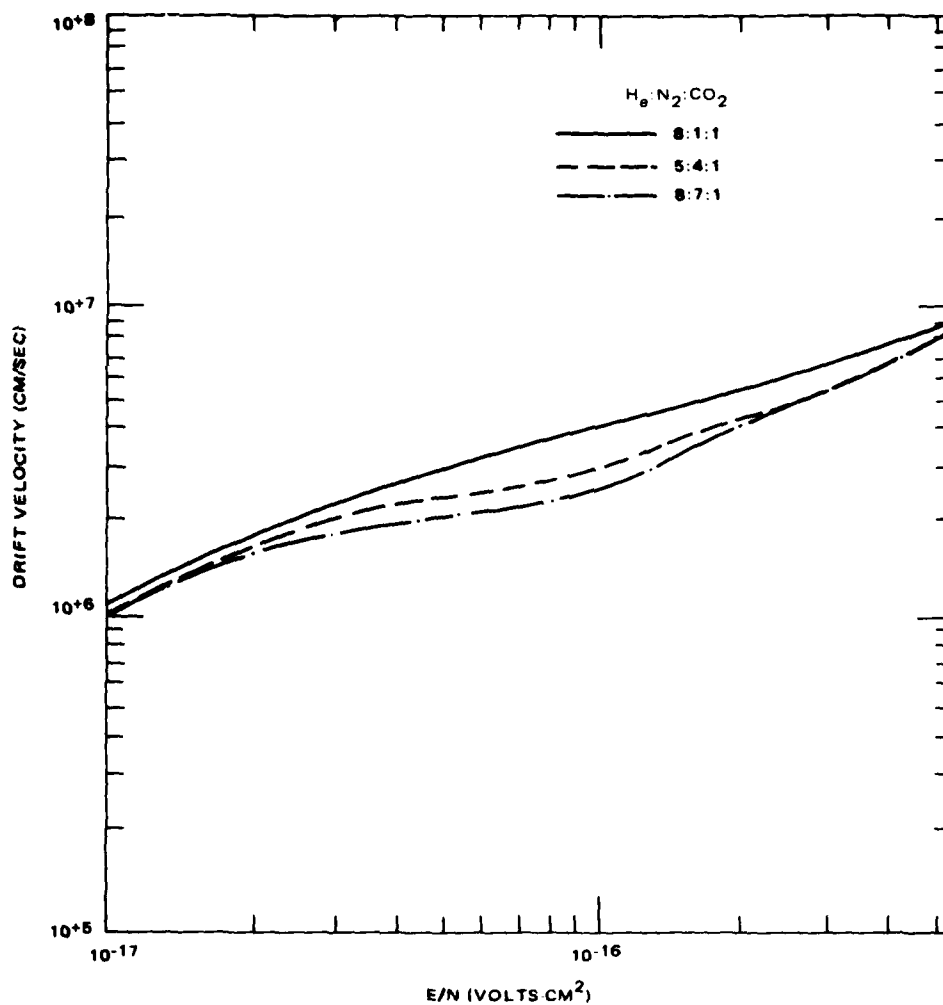


Figure 8. Electron drift velocity vs  $E/N$  for various gas mixes (from references 3 and 4).

## DETERMINATION OF $N_e$

Once  $P_{\ell h}$  and  $V_{rms}$  are determined, the electron number density,  $N_e$ , during the pulse can be estimated using the relation:

$$\eta_d P_{\ell h} / V_{rms} = I_{rms} = q N_e v_d A \quad (10)$$

where  $I_{rms}$  is the rms discharge current density,  $q$  is the electron charge,  $v_d$  is the average electron drift velocity, and  $A$  is the discharge area.

The value of  $v_d$  will vary with  $E/N$  and gas mix since on the molecular level it involves the effect of collisions of electrons and molecules having different energies and collision cross-sections. The relationship of  $v_d$  to  $E/N$  can be calculated using the Boltzmann transport equation in conjunction with the collision cross-sections for the various gas species. Figure 8 illustrates the dependence of  $v_d$  on  $E/N$  for various gas mixes.

Using the previous laser head data of  $V_{rms} = 555$  volts and assuming  $v_d = 10^7$  cm/sec and  $A = 0.2$  cm  $\times$  19 cm  $\approx$  3.8 cm<sup>2</sup> we obtain  $N_e = 5.5 \times 10^{11}$  cm<sup>-3</sup>. The assumption is also implicitly made that  $N_e$  will not change appreciably per half cycle of the rf power input and it is also assumed that the gas temperature is approximately 350°K such that  $N \sim 2.8 \times 10^{18}$  cm<sup>-3</sup>.

## ELECTRICAL SUMMARY

The preceding discussion is sufficient in describing the basic electrical characteristics of rf pumped lasers. The analysis has ignored standing wave effects which occur in electrically long devices or very high frequency devices (greater than 150 MHz). The parametric gain and output power data presented later in the report will not include corresponding parametric electrical data such as the variation of  $R_g$  with discharge condition as this data was not recorded due to the fact that this data was not contractually required and the tediousness of the calculations did not warrant the investment of analysis time.

## LASER CHARACTERISTICS MODEL

The following discussion will deal with a brief overview of CO<sub>2</sub> laser kinetics. A detailed analysis of the coupled discharge, gas thermodynamics, and laser kinetics has not been attempted due to the extreme complexity of the problem. Instead a simplified analysis of the pulsed laser performance will be discussed.

### LASER KINETICS MODEL

A summary of the more important CO<sub>2</sub> laser kinetics data and laser equations will be discussed at this time. Unless otherwise noted, this discussion is based on Reference 3.

The total stored vibrational energy above thermal equilibrium,  $E_s$ , in a mixture of CO<sub>2</sub> and N<sub>2</sub> is given by:

$$E_s \approx N(\phi_{\text{CO}_2} + \phi_{\text{N}_2})\epsilon_{001}\left(\frac{A}{1-A}\right) \text{ Joules/cm}^3 \quad (11)$$

where

- $N$  = the total number density of all gas species in  $\text{cm}^{-3}$
- $\phi_{\text{CO}_2}$  = the molar fraction of CO<sub>2</sub> in the gas mix
- $\phi_{\text{N}_2}$  = the molar fraction of N<sub>2</sub> in the gas mix
- $A$  = the Boltzmann factor of the upper laser level
- $\epsilon_{001}$  = the characteristic energy of the upper laser level which equals  $4.66 \times 10^{-20}$  Joules

The small signal 10  $\mu$ band gain for a CO<sub>2</sub> laser mixture is given by:

$$g_o = N\phi_{CO_2} (1-A)(1-B)(1-B^{1/2})^2 \sigma (g_{001, J^A} - g_{100, J^B}) \quad (12)$$

where

$B'$  = the Boltzmann factor for the lower 10  $\mu$ band laser level

$B$  = the characteristic Boltzmann factor of the symmetric stretch mode of the CO<sub>2</sub> molecules  $B = B'e^{(74.8/T_g)}$

$\sigma$  = the optical cross-section for the transition in cm<sup>2</sup>

$g_{nlm, J}$  = the population fraction of the vibrational level nlm, in a particular rotational level, J

J = the rotational quantum number of the upper laser level

J' = the rotational quantum number of the lower laser level

and also noting that  $B = e^{-1922/T_g}$  where  $T_g$  equals the gas temperature in °K.

The optical cross-section for the 10.6 $\mu$  transition in a CO<sub>2</sub>, N<sub>2</sub>, and He mixture is given by:

$$\sigma = \frac{4.08 \times 10^{-17} (T_g)^{1/2}}{P (\phi_{CO_2} + 0.87 \phi_{N_2} + 0.64 \phi_{He})} \quad (13)$$

where P is the total gas pressure in Torr.

The rotational population fraction,  $g_{nlm, K}$ , is given by:

$$g_{nlm, K} = \frac{2B_{nlm}}{kT_g} (2K + 1) e^{-B_{nlm} K(K+1)/kT_g} \quad (14)$$

where

k = Boltzmann's constant  $1.38 \times 10^{-23}$  Joules/°K

$B_{nlm}$  = the characteristic rotational energy of the vibrational mode, nlm

K = the rotational quantum number of a specific vibrational mode

and also noting that  $B_{001} = 7.685 \times 10^{-24}$  Joules and  $B_{100} = 7.746 \times 10^{-24}$  Joules.

For gas pressure in excess of 20 Torr, the laser medium is predominately pressure broadened such that the steady-state saturated gain,  $g$ , is given by the expression:

$$g = \frac{g_0}{1 + I/I_s} \quad (15)$$

where

$I$  = the optical intensity in  $W/cm^2$

$I_s$  = the saturation intensity in  $W/cm^2$

The  $10.6\mu$  saturation intensity is defined by the equation:

$$I_s = \frac{h\nu}{g_{001.19} \sigma \tau} \quad (16)$$

where

$h$  = Planck's constant =  $6.626 \times 10^{-34}$  Joule-sec

$\nu$  = the optical frequency in Hz

$\tau$  = the characteristic decay time of asymmetric stretch mode in  $\mu\text{sec}$

The upper level decay time,  $\tau$ , is a function of gas mix, pressure, and temperature when molecular collisions dominate and is given by the equation:

$$\frac{1}{\tau} = \bar{P} \sum_i \frac{\phi_i}{\tau_i} \quad (17)$$

where

$\bar{P}$  = gas pressure in atm.

$\phi_i$  = the molar fraction of the specie

$\tau_i$  = the decay time due to the ith specie in atm-sec.

Figure 9 gives values of  $\tau_i$  versus temperature for  $\text{CO}_2$ ,  $\text{N}_2$ , and He.

For example, calculated values for these various parameters for an 8:1:1 ( $\text{He}:\text{N}_2:\text{CO}_2$ ) mix at 100 Torr and  $350^\circ\text{K}$  with  $A = 0.2$  for the  $10.6\mu$  transition are given below:

$$\begin{aligned} N &= 2.76 \times 10^{18} / \text{cm}^3 \\ \nu &= 2.83 \times 10^{13} \text{ Hz} \\ \phi_{\text{CO}_2} &= 0.10 \\ \phi_{\text{N}_2} &= 0.10 \\ \phi_{\text{He}} &= 0.80 \\ E_s &= 6.43 \times 10^{-3} \text{ J/cm}^3 \\ g_{001,19} &= 6.78 \times 10^{-2} \\ g_{100,20} &= 6.71 \times 10^{-2} \\ \tau &= 79 \mu\text{sec} \\ I_s &= 320 \text{ W/cm}^2 \\ \sigma &= 1.09 \times 10^{-17} \text{ cm}^2 \\ B &= 4.12 \times 10^{-3} \\ B' &= 3.33 \times 10^{-3} \\ g_0 &= 2.8 \text{ percent/cm} \end{aligned}$$

#### POWER OUTPUT EFFICIENCY

The pulsed rf laser used in these experiments tended to produce a gain switched output spike followed by a much lower power and temporarily long tail. In many respects the output resembles that of a Q-switched laser. In  $\text{CO}_2$  lasers, even in the absence of  $\text{N}_2$  or  $\text{CO}$  in the mix, the energy in higher lying levels tends to decay back to the upper laser level in times comparable to several cavity lifetimes such that the pulsewidth will be larger than predicted theoretically. The cavity lifetime is defined by the equation:<sup>5</sup>

$$t_c = \frac{2l}{c (L - \ln(R))} \quad (18)$$

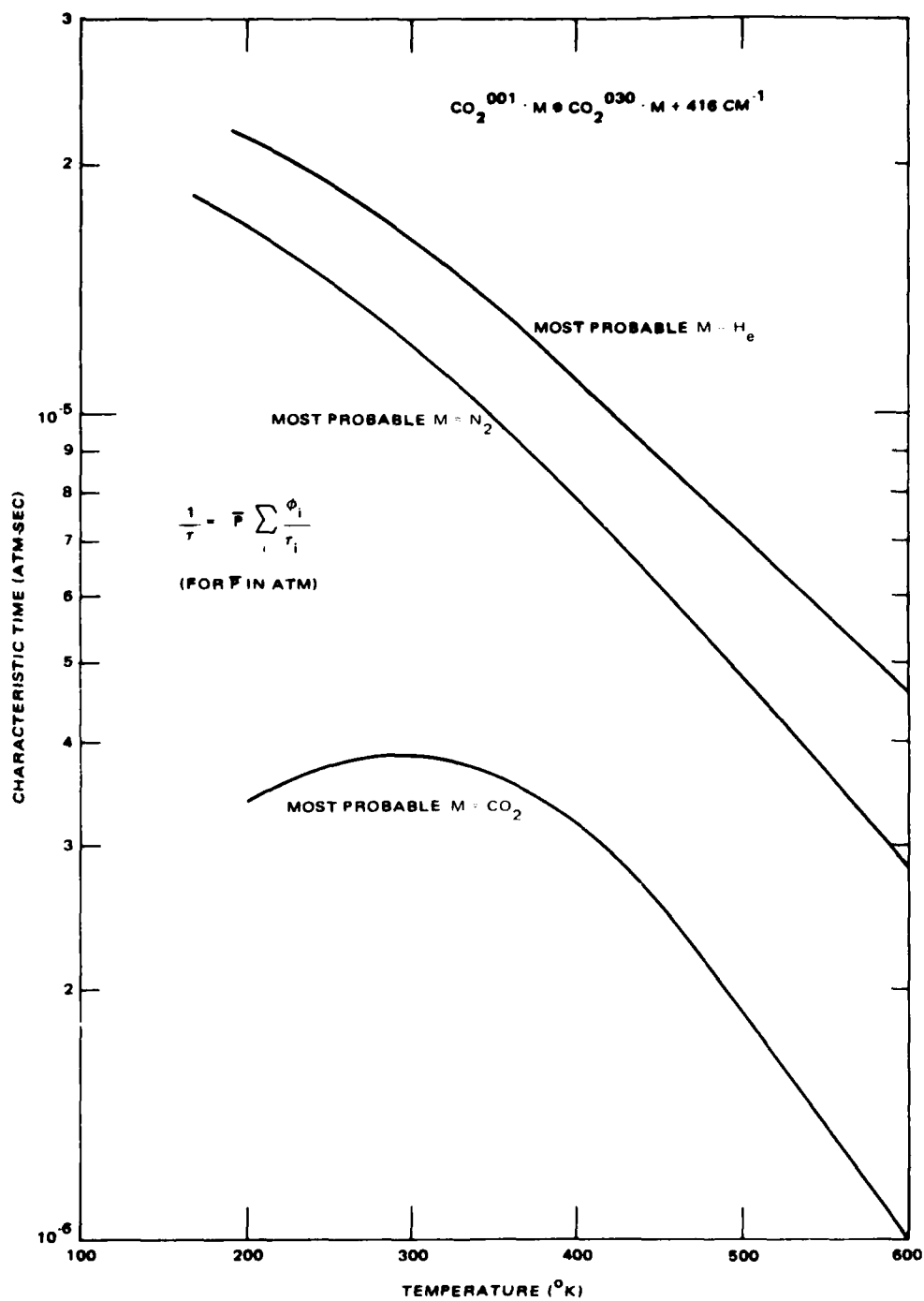


Figure 9. The characteristic decay time,  $\tau_i$ , for various collision partners (from reference 3).

where

- $c$  = the speed of light  $= 2.998 \times 10^{10}$  cm/sec
- $\ell$  = the cavity length in cm
- $R$  = the product of the power reflectivities of the resonator mirrors
- $L$  = the total round-trip intensity losses of the laser

The threshold gain of the laser is defined by:

$$g_{th} = \frac{1}{c t_c} \quad (19)$$

For cases where  $g_o/g_{th}$  is large ( $>4$ ) the theoretical pulsewidth of the gain-switched pulse is on the order of several cavity lifetimes and 50 percent or more inversion energy is extracted in the power pulse. A discussion of the characteristics of Q-switched lasers is given in Reference 5.

For the purposes of this discussion, we will analyze the efficiency of the pulsed rf laser in terms of the total energy extracted in the power spike and tail as compared to the input energy. The total energy stored in the upper laser levels is given by Equation (11) and by:

$$E_s \cong \eta_p \tau_p \eta_d P_{\ell h} \quad (20)$$

where

- $\eta_p$  = the discharge pumping efficiency to the upper laser levels
- $\eta_d P_{\ell h}$  = the rf power delivered to the discharge
- $\tau_p$  = the power input pulsewidth in  $\mu$ sec

and where the implicit assumption is made that  $\tau_p \ll \tau$  where  $\tau$  is the deactivation time of the upper level vibrational mode defined by Equation (17).

(See References 3 and 4 for values of  $\eta_p$  versus  $E/N$  for several gas mixes.)

The total extracted energy in the output power spike can be defined by the following equation:

$$E_p = \eta_q \eta_e \eta_r E_s \left[ \frac{\phi_{CO_2}}{\phi_{N_2} + \phi_{CO_2}} \right] \quad (21)$$

where

$\eta_q$  = the quantum efficiency of the  $10.6\mu$  transition = 0.41

$\eta_e$  = the extraction efficiency

$\eta_r$  = the resonator efficiency

where  $\eta_r$  is defined by the equation:

$$\eta_r = \frac{(1 - R)}{(1 - R) + L} \quad (22)$$

The value of  $\eta_e$  is in general dependent on the laser gas mix, laser pulsewidth, and the ratio of  $g_o/g_{th}$ .  $\eta_e$  can approach unity in value for gain-switched pulsewidths which are much shorter than the upper level lifetime but longer than the lower level lifetime and where  $g_o/g_{th}$  is large (greater than 4.0). Normally the lower level does not meet this requirement unless  $H_2O$  is added to the laser mix to increase the lower level deactivation rate. For cases in which the pulsewidth is shorter than both the upper and lower level lifetimes,  $\eta_e$  will approach the approximate value:

$$\eta_e \approx \frac{1}{2} \left( \frac{g_o - g_{th}}{g_o} \right) \quad (23)$$

The total round trip loss,  $L$ , of the laser resonator is a combination of lumped and distributed losses. For example, bore coupling losses (see Reference 6) and distributed waveguide losses (see References 7 and 8) will occur. For the particular design used in these studies, the coupling loss is about 2 percent and the waveguide loss is estimated to be about 2 percent.

The total efficiency of the laser gain-switched pulse,  $\eta_l$ , is thus given by the expression:

$$\eta_l = \frac{E_p}{\tau_p P_{th}} = \eta_d \eta_q \eta_p \eta_r \eta_e \left[ \frac{\phi_{CO_2}}{\phi_{N_2} + \phi_{CO_2}} \right] \quad (24)$$

For example, consider an 8:1:1 laser mix with  $L = 0.03$ ,  $R = 0.90$ ,  $l = 20$  cm, and  $g_0 = 1.5$  percent/cm. One then calculates using  $\eta_d = 0.93$ ,  $\eta_q = 0.41$ , and assuming  $\eta_p = 0.30$ :

$$t_c = 9.9 \text{ nsec}$$

$$P_{th} = 0.34 \text{ percent/cm}$$

$$\eta_r = 0.77$$

$$\eta_e = 0.39$$

$$(\phi_{CO_2})/(\phi_{N_2} + \phi_{CO_2}) = 0.5$$

$$\eta_l \approx 0.017$$

$$E_p = 0.062 E_s$$

These numbers are typical for the high loss external resonator used in these experiments. Improved design will increase the expected overall efficiency especially by improvement in  $\eta_r$  and  $\eta_d$ .

For mixtures containing  $N_2$ , the power output tail will contain the energy stored in the  $N_2$  molecule while the leading spike will contain the energy stored in the  $CO_2$  upper laser level mode only. The total laser efficiency,  $\eta_t$ , will be equal to the sum of the energy in the power spike and in the tail divided by the total power delivered to the laser head and is approximately equal to:

$$\eta_t = \eta_d \eta_q \eta_p \eta_r \eta_e \quad (25)$$

where experimentally  $\eta_t$  has been observed to be as high as 15 percent.

#### GAIN-SWITCHED PULSE DELAY TIME, $\tau_{gs}$

The typical laser power output from the pulsed rf laser consists of a gain-switched pulse followed by a long decay tail. The gain-switched pulse occurs several microseconds after the start of the rf power input to the discharge. This pulse delay time,  $\tau_{gs}$ , can be estimated in the following manner.

Assuming that the temporal gain profile is characterized by a linear ramp within the first few microseconds of discharge, then the gain versus time,  $g(t)$ , at flux levels much less than the saturation flux is approximately given by:

$$g(t) = at - g_{th} \quad (26)$$

where  $(a)$  is the rate of change in small signal gain versus time at  $t = 0$  in  $\text{cm}^{-1}\text{sec}^{-1}$ . This equation is a good approximation whenever  $t > \tau_{gs}$  and  $\tau_{gs} \ll \tau$  where  $\tau$  is the previously defined upper level decay time.

The derivative of laser flux versus time,  $dI/dt$ , is approximated by:

$$\frac{dI}{dt} = I g(t) \quad (27)$$

integrating,

$$\int_{I_0}^{I_p} \frac{dI}{I} = c \int_0^{\tau_{gs}} (at - g_{th}) dt \quad (28)$$

where we implicitly assume  $\tau_p \geq \tau_{gs}$  and where,

$I_p$  = the intensity of the gain-switched pulse

$I_0$  = the intensity of one photon in the mode which eventually becomes the gain-switched pulse

Two assumptions are made here. We assume that within nanoseconds after  $g(t)$  reaches  $g_{th}$  that the initial photon flux,  $I_o$ , is reached. Also assumed is that the gain-switched spike intensity,  $I_p$ , is reached within tens of nanoseconds after  $I$  reaches the saturation flux,  $I_s$ . Thus saturation effects on the gain are ignored. Both these assumptions are valid for the pulsed rf laser.

The power in the initial photon flux,  $P_o$ , is given by:

$$P_o = \frac{ch\nu}{l}$$

where,

$\nu$  = the laser frequency

$l$  = the resonator length

$P_o = 1.1 \times 10^{-8}$  for  $l = 20$  cm and  $\lambda = 10.6 \mu m$ .

The pulse laser output power,  $P_p$ , is given by:

$$P_p = I_p A_r \quad (29)$$

where  $A_r$  is the area of the mode and

$$A_r \approx \frac{\pi(0.70 d)^2}{4} \quad (30)$$

where  $d$  = the bore size.

Substituting into equation (28) one obtains:

$$\ln\left(\frac{P_p}{P_o}\right) = c\left(\frac{a \tau_{gs}^2}{2} - g_{th} \tau_{gs}\right) \quad (31)$$

Solving the quadratic for  $\tau_{gs}$ :

$$\tau_{gs} = \frac{g_{th} + \sqrt{g_{th}^2 + (2a/c) \ln (P_p/P_o)}}{a} \quad (32)$$

Analysis of the gain data indicates typical values of (a) in the  $2000 \text{ cm}^{-1} \text{ sec}^{-1}$  to  $3000 \text{ cm}^{-1} \text{ sec}^{-1}$  range depending on the conditions of the discharge and the gas mix. As an example, for the condition:

$$\begin{aligned} g_{th} &= 4.0 \times 10^{-3} \\ a &= 2200 \text{ cm}^{-1} \text{ sec}^{-1} \\ P_p &= 500 \text{ W} \end{aligned}$$

then

$$\tau_{gs} = 3.8 \text{ } \mu\text{sec}$$

which is typical of the actual  $\tau_{gs}$  seen in the experimental data.

The preceding discussion has looked at the more important aspects of the laser kinetics and expected performance under the assumptions previously outlined. This discussion is not meant to be a rigorous analysis of the problem. It is intended as a guide to the general understanding of the data to be presented in the next section.

## SEALED LASER EXPERIMENTAL RESULTS

Peak small signal gain and extracted laser output power data was obtained for the pulsed rf waveguide laser for both sealed and flowing gas conditions. The discussion in this section will be primarily devoted to the sealed data whereas the flowing gas data from the Phase I report is appended to this report (see Appendix A).

To minimize the amount of data, the total gas pressure was set to 125 Torr. Laser power output was optimized in the 2.5 mm bore device at 125 Torr total pressure for most of the gas mixes tested. Lower pressure operation in general lowered the output power in the gain switched spike whereas higher pressure operation led to discharge instability at the 2.0 kW input power level. Most of the data was taken at 1.0 kHz repetition rate since this repetition rate was optimal in terms of laser performance for the gas mixes tested.

### SEALED GAIN DATA

#### Experimental Setup and Discussion

Figure 10 illustrates the experimental arrangement for the sealed small signal gain experiments. The beam from a Sylvania  $\text{CO}_2$  stabilized laser was tuned to the line center of the  $10.6\mu$  P(20) transition and attenuated to 5 mW. The beam then reflected from a mirror and was apertured before entering into the waveguide bore. The beam passing out of the waveguide bore was imaged on the HgCdTe 10 MHz detector by placing a ZnSe lens of  $f = 7.5$  cm at twice this distance from the laser bore and the detector thereby eliminating steering effects of the pulsed heated gas. A manually operated blocking

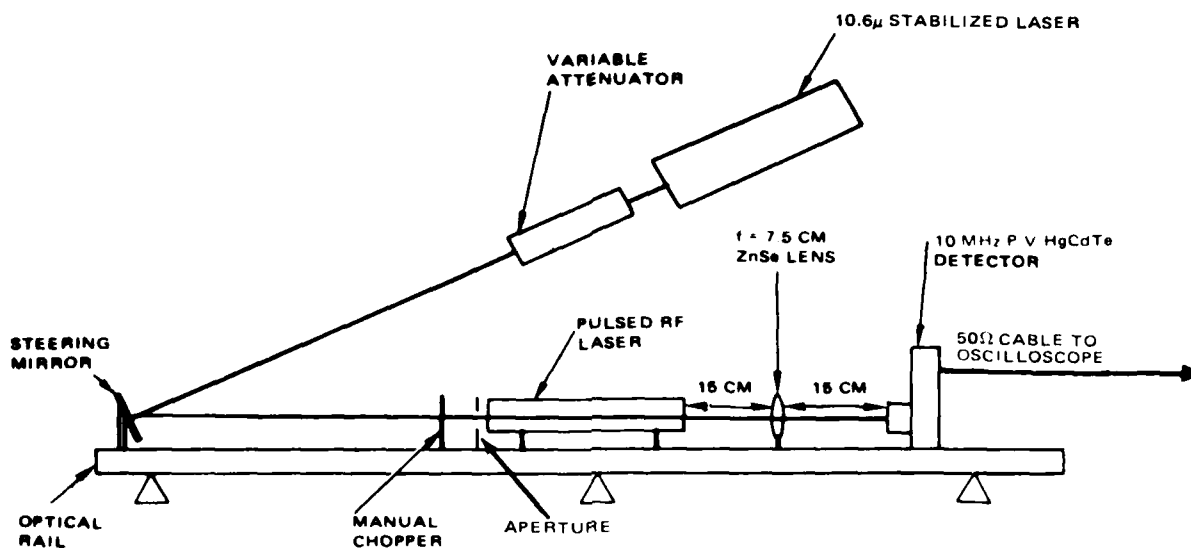


Figure 10. Small signal gain experimental apparatus

screen was placed directly in front of pulsed device so that a zero level reading could be obtained for the dc coupled detector by blocking the probe beam. The detector was connected by a 50 ohm line to a 50 ohm oscilloscope in parallel to a 51 ohm termination. The other channel of the scope was used to record the attenuated forward rf voltage signal.

### Results

Sealed data was obtained on the 8:1:1, 5:1:1, and 5:0:1 He:N<sub>2</sub>:CO<sub>2</sub> gas mixes. N<sub>2</sub> was added to these mixes to improve the discharge stability and increase the laser efficiency. Only small signal gain was measured and no saturated data was taken. The data will be presented in tabular form using the following variables to describe the measurement data:

- $P_{ph}$  = average pulse power into the lower head in kW
- $\tau_p$  = pulsewidth of the forward power pulse in  $\mu$ sec
- $f_p$  = the pulse repetition rate in kHz
- $g_p$  = the peak measured small signal gain in  $\text{cm}^{-1}$
- $\tau_d$  = the characteristic decay time of the gain after reaching  $g_p$  in  $\mu$ sec

This reduced data is presented in Table 1 and Figure 11. Figures 12 and 13 illustrate the actual data taken for various experimental conditions. The small signal gain versus time is illustrated in these figures and is determined by the lower three traces of each photo. The upper of the three traces is the detector signal with input power pulse to the pulsed laser. The next lower line is the detector signal without power pulse to the pulsed laser. The lowest line is the zero level of the detector. Thus these three traces determine the small signal gain of the laser medium versus time. The uppermost trace is the attenuated envelope of the forward voltage pulse (-63.6 dB attenuation).

The gases used in these measurements were obtained from three premixed ultrapure bottles of 3:1:1 (He:N<sub>2</sub>:CO<sub>2</sub>), 8:1:1, and 3:0:1 + 1.0% H<sub>2</sub>O with additional bottles of X<sub>e</sub> and ultrapure N<sub>2</sub> being added to these mixes to obtain variations on the premixed gases. This notation (i.e., 84% (3:1:1) + 10% X<sub>e</sub>) has been adopted so that comparison with the flow gas data in Appendix A can be more easily visualized.

There are several notable aspects to this data. For  $\tau_p$  greater than 5  $\mu$ sec the 84% (3:1:1) + 16% X<sub>e</sub> mix had the highest  $g_p$  followed by the 80% (3:0:1) + 12.8% X<sub>e</sub> + 6.4% N<sub>2</sub> + 0.8% H<sub>2</sub>O, 86.3% (3:0:1) + 12.8% X<sub>e</sub> + 0.9% H<sub>2</sub>O, and the 84% (8:1:1) + 16% X<sub>e</sub> mixes respectively. Thus the higher the N<sub>2</sub> concentration, the higher the  $g_p$  with the exception of the 84% (8:1:1) + 16% X<sub>e</sub> mix which at 8.4% N<sub>2</sub> content had the lowest  $g_p$  at any  $\tau_p$  when compared with the other mixes. As  $\tau_p$  is decreased to 3.0  $\mu$ sec, the highest  $g_p$  switches from the 84% (3:1:1) + 16% X<sub>e</sub> to the lower N<sub>2</sub> concentration mix of 83% (3:0:1) + 12.8% N<sub>2</sub> + 6.4% N<sub>2</sub> + 1.0% H<sub>2</sub>O. The addition of H<sub>2</sub>O to the mix was found to help increase the power in the gain-switched output power spike. This was assumed to be due to the increased deactivation rate of the lower laser level. Also the decay tails generally tended to be longer with increasing N<sub>2</sub>/CO<sub>2</sub> ratios and shorter as  $\tau_p$  was increased (due to the increased temperature increasing the upper level decay rate).

TABLE 1. SEALED SMALL SIGNAL GAIN DATA

Gas Mix	$f_p$ (kHz)	$\tau_p$ (usec)	$\tau_d$ (usec)	$g_p$ ( $^{10}/cm$ )	Comments
A	1.0	3.0	140	0.91	Gas Mix A = 84% (8:1:1) + 16% Xe
A	1.0	6.0	120	1.36	
A	1.0	10.0	105	1.46	
B	1.0	3.0	120	1.31	Gas Mix B = 84% (3:1:1) + 16% Xe
B	1.0	6.0	100	1.88	
B	1.0	10.0	70	2.28	
C	1.0	3.0	75	1.00	Gas Mix C = 86.3% (3:0:1) + 12.8% Xe + 0.9% H <sub>2</sub> O
C	1.0	6.0	70	1.41	
C	1.0	10.0	50	1.57	
D	1.0	3.0	65	1.37	Gas Mix D 80% (3:0:1) + 12.8% Xe + 6.4% N <sub>2</sub> + 0.8% H <sub>2</sub> O
D	1.0	6.0	60	1.76	
D	1.0	10.0	50	1.93	
C	0.5	3.0	—	0.97	NOTE: All data with P = 125 Torr P <sub>th</sub> = 2.0 kW
C	1.5	3.0	—	0.96	
C	2.0	3.0	—	0.92	
C	2.5	3.0	—	0.91	
C	3.0	3.0	—	0.92	
C	3.5	3.0	—	0.81	

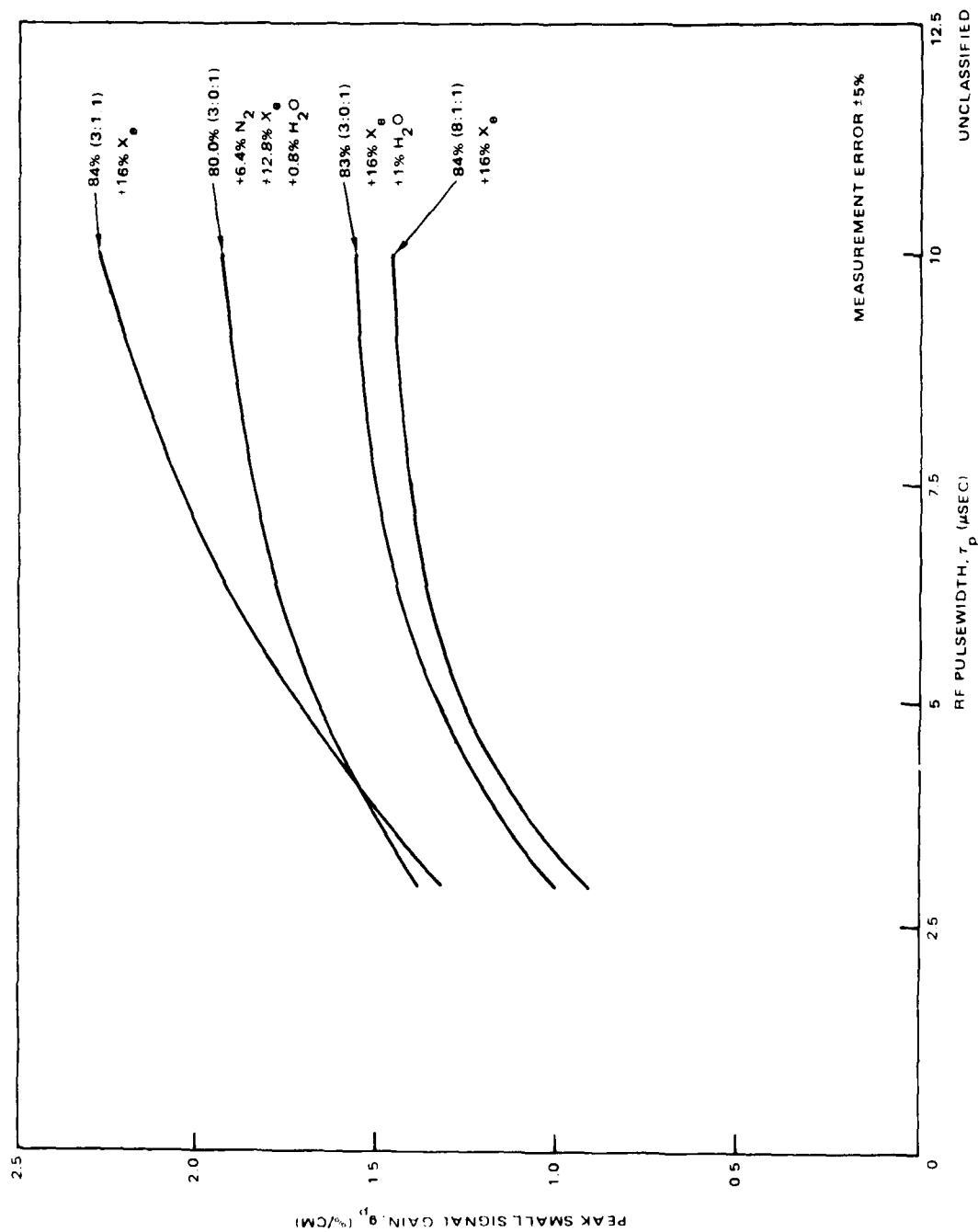
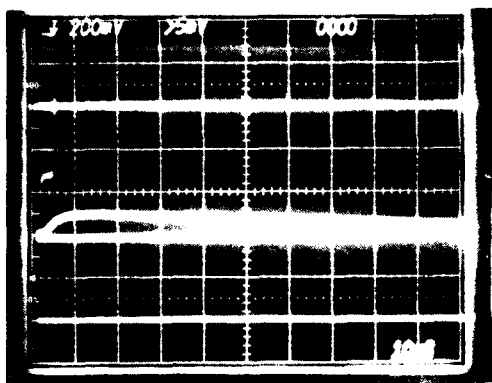
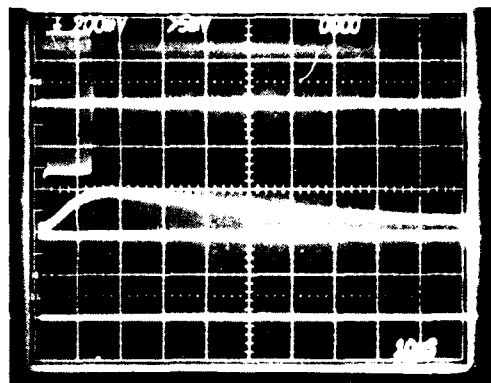


Figure 11.  $g_p$  versus  $\tau_p$  for various gas mixes at  $P = 125$  Torr,  $P_h = 2.0$  kW, and  $f_p = 1.0$  kHz.



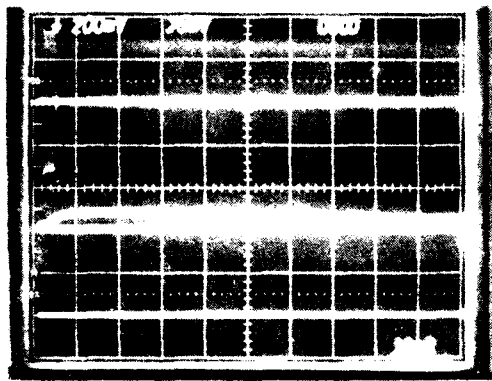
MIX 84 (3.1.1) 16 $\times$  X<sub>p</sub>

$P_{ch} = 2.0 \text{ kW}$   $t_d \sim 120 \mu\text{SEC}$   
 $P = 125 \text{ TORR}$   $f_p = 1.0 \text{ kHz}$   
 $t_p = 3.0 \mu\text{SEC}$   $q_p = 0.013 \text{ cm}$



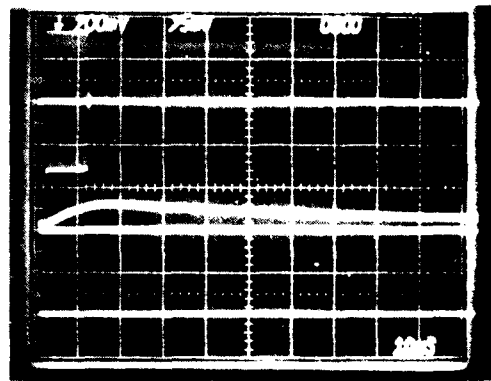
MIX 84 (3.1.1) 16 $\times$  X<sub>p</sub>

$P_{ch} = 2.0 \text{ kW}$   $t_d \sim 120 \mu\text{SEC}$   
 $P = 125 \text{ TORR}$   $f_p = 1.0 \text{ kHz}$   
 $t_p = 3.0 \mu\text{SEC}$   $q_p = 0.013 \text{ cm}$



MIX 84 (3.1.1) 16 $\times$  X<sub>p</sub>

$P_{ch} = 2.0 \text{ kW}$   $t_d \sim 130 \mu\text{SEC}$   
 $P = 125 \text{ TORR}$   $f_p = 1.0 \text{ kHz}$   
 $t_p = 3.0 \mu\text{SEC}$   $q_p = 0.009 \text{ cm}$

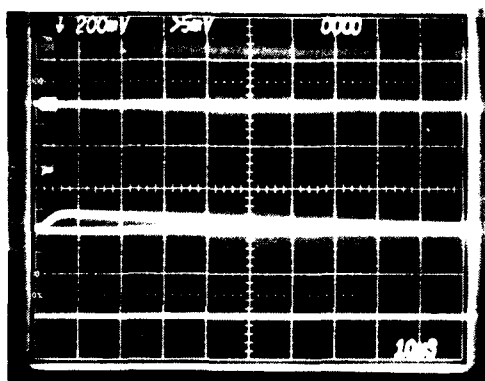


MIX 84 (3.1.1) 16 $\times$  X<sub>p</sub>

$P_{ch} = 2.0 \text{ kW}$   $t_d \sim 100 \mu\text{SEC}$   
 $P = 125 \text{ TORR}$   $f_p = 1.0 \text{ kHz}$   
 $t_p = 3.0 \mu\text{SEC}$   $q_p = 0.013 \text{ cm}$

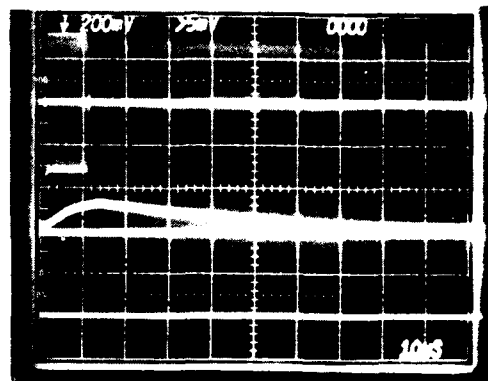
NOV 1964

Figure 12. Typical small signal gain data for 1.1 and 8.1 Torr mixtures with X<sub>p</sub>.



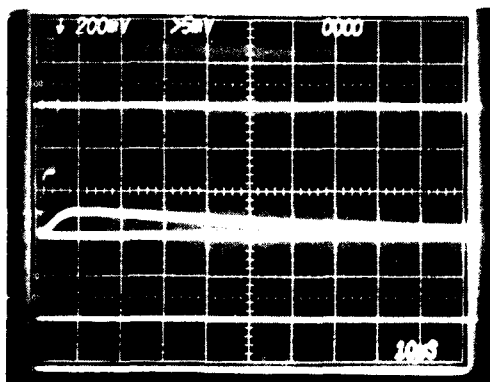
MIX: 83% (3.0:1) + 16%  $X_p$  + 1.0%  $H_2O$

$P_{ch}$  2.0 kW       $\tau_d \sim 75 \mu\text{SEC}$   
 $P$  125 TORR       $f_p$  1.0 kHz  
 $\tau_p$  3.0  $\mu\text{SEC}$        $q_p$  0.010/cm



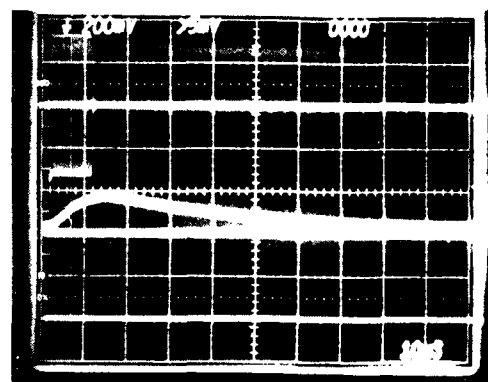
MIX: 83% (3.0:1) + 16%  $X_p$  + 1.0%  $H_2O$

$P_{ch}$  2.0 kW       $\tau_d \sim 50 \mu\text{SEC}$   
 $P$  125 TORR       $f_p$  1.0 kHz  
 $\tau_p$  10  $\mu\text{SEC}$        $q_p$  0.016/cm



MIX: 80% (3.0:1) + 12.8%  $X_p$  + 6.4%  $N_2$  + 0.8%  $H_2O$

$P_{ch}$  2.0 kW       $\tau_d \sim 65 \mu\text{SEC}$   
 $P$  125 TORR       $f_p$  1.0 kHz  
 $\tau_p$  3.0  $\mu\text{SEC}$        $q_p$  0.014/cm



MIX: 80% (3.0:1) + 12.8%  $X_p$  + 6.4%  $N_2$  + 0.8%  $H_2O$

$P_{ch}$  2.0 kW       $\tau_d \sim 50 \mu\text{SEC}$   
 $P$  125 TORR       $f_p$  1.0 kHz  
 $\tau_p$  10  $\mu\text{SEC}$        $q_p$  0.014/cm

UNCLASSIFIED

Figure 13. Typical small signal gain data for (3.0:1)  $X_p$  as  $H_2O$  and  $X_p$  with and without  $N_2$

The 80% (3:0:1) + 12.8%  $N_e$  + 6.4%  $N_2$  + 1.0%  $H_2O$  appears to have the largest increase in  $g_p$  with  $\tau_p$  for  $\tau_p$  less than about 4  $\mu$ sec as compared to the other three mixes. This mix also produced the largest gain-switched spike of the four mixes for  $\tau_{gs}$  less than 4  $\mu$ sec at a given rf input power.

Comparison of the sealed small signal gain data to the flowing gas small signal gain data in Appendix A indicates that the flowing gas device had higher gains in general even without  $N_e$  in the gas mix as compared to the sealed off device. This is probably primarily due to lower temperatures in the flowing gas device.

## SEALED POWER OUTPUT DATA

### Experimental Setup and Discussion

Figure 14 illustrates the experimental arrangement for the sealed power output measurements. The pulsed rf laser was operated with internal optics as opposed to the arrangement used in flowing gas experiments in which external optics were employed. The resonator optics were mounted to the ends of the laser shell by compression against o-ring gas seals. The resonators were aligned by rocking the optics on these o-rings.

The average laser output power was monitored with a Coherent Radiation No. 210 power meter. The actual pulse shape of the laser output was monitored by observing the direct radiation with a calibrated Moletron

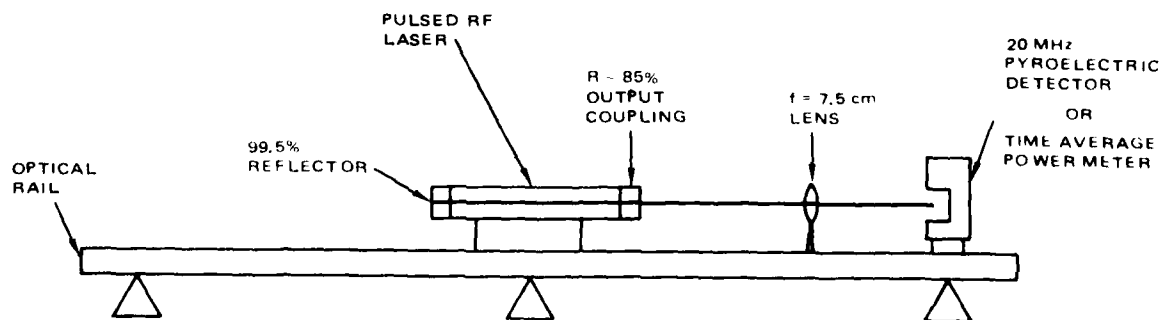


Figure 14. Sealed power output experimental apparatus.

20 MHz pyroelectric detector and amplifier combination. The detector and amplifier were calibrated to 1.0 mV/watt. The detector amplifier was terminated into an oscilloscope. The oscilloscope was 20 MHz band-limited to prevent the 150 MHz rf noise from being displayed. A second 50 ohm channel on the 400 MHz oscilloscope was used to record the attenuated forward rf voltage waveform.

As in the small signal gain experiments, the gases used in these measurements were obtained from three premixed ultrapure bottles of 3:1:1 (He:N<sub>2</sub>:CO<sub>2</sub>), 8:1:1, and 3:0:1 + 1% H<sub>2</sub>O with additional bottles of X<sub>e</sub> and ultrapure N<sub>2</sub> being added to these mixes to obtain variations on the premixed gases.

### Results

Sealed data was obtained on the 8:1:1, 3:1:1, and 3:0:1 (He:N<sub>2</sub>:CO<sub>2</sub>) + 1.0% H<sub>2</sub>O gas mixes. X<sub>e</sub> was added to these mixes to improve the discharge stability and increase the laser efficiency. The H<sub>2</sub>O added to the 3:0:1 mix tended to optimize the gain-switched pulse output power. The data is presented in Table 2 using the same nomenclature as Table 1 with the added measurement variables:

$P_p$  = the peak laser output power in watts

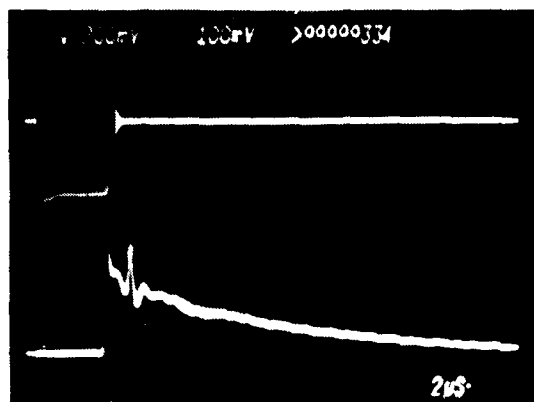
$P_{ave}$  = the average laser output power in watts

Figures 15 and 16 illustrate some of the actual laser output data for various experimental conditions. The lower trace in each photo is the pyroelectric signal of the laser output power pulse while the upper trace represents the attenuated forward voltage pulse. Reduced data is presented in Figures 17 through 21.

Figure 17 is a graph of  $P_{ave}$  versus  $\tau_p$  for various gas mixes. Note that the mixes tested have almost a linear change in  $P_{ave}$  with  $\tau_p$  and that the 84% (3:1:1) + 16% X<sub>e</sub> had the highest  $P_{ave}$  for any  $\tau_p$  when compared with the other mixes.

TABLE 2. SEALED POWER OUTPUT DATA

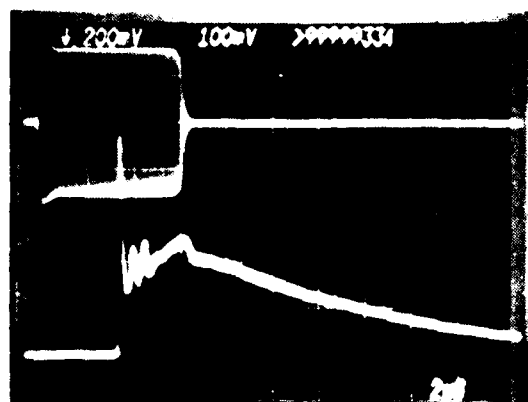
Gas Mix	$f_p$ (kHz)	$\tau_p$ ( $\mu$ sec)	$P_p$ (watts)	$P_{ave}$ (watts)	Comments
A	1.0	3.0	190	0.43	Gas Mix A = 84% (8:1:1) + 16% $X_e$
A	1.0	6.0	340	1.20	
A	1.0	10.0	340	2.20	
B	1.0	3.0	600	0.90	Gas Mix B = 84% (3:1:1) + 16% $X_e$
B	1.0	6.0	460	1.80	
B	1.0	10.0	—	3.00	
C	1.0	3.0	470	0.19	Gas Mix C = 86.3% (3:0:1) + 12.8% $X_e$ + 0.9% $H_2O$
C	1.0	6.0	510	0.60	
C	1.0	10.0	520	1.15	
D	1.0	3.0	600	0.72	Gas Mix D = 80% (3:0:1) + 12.8% $X_e$ + 6.4% $N_2$ + 0.8% $H_2O$
D	1.0	6.0	610	1.50	
D	1.0	10.0	—	2.55	
C	0.5	3.0	400	0.10	Gas Mix E = 98.8% (3:0:1) + 1.2% $H_2O$
C	1.5	3.0	390	0.26	
C	2.0	3.0	380	0.35	
C	2.5	3.0	400	0.43	
C	3.0	3.0	360	0.50	
C	3.5	3.0	260	0.46	
E	1.0	3.0	290	0.10	NOTE: All data with $P = 125$ Torr $P_{th} = 2.0$ kW
E	1.0	6.0	370	0.36	
E	1.0	10.0	370	0.54	



MIX 84% (3:1:1) + 16%  $X_e$

$P_{\text{ch}} = 2.0 \text{ kW}$      $t_p = 3.0 \mu\text{SEC}$      $f_p = 1.0 \text{ kHz}$

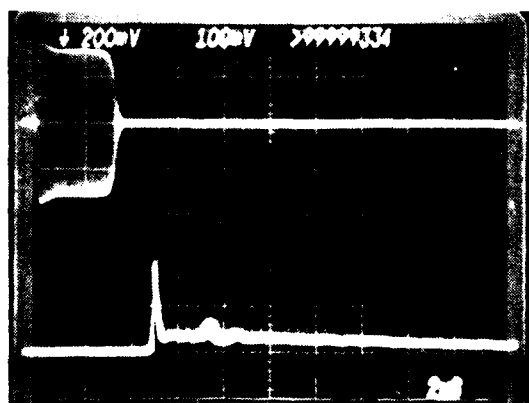
$R = 0.85$      $P = 125 \text{ TORR}$      $P_p \sim 600\text{W}$



MIX 84% (3:1:1) + 16%  $X_e$

$P_{\text{ch}} = 2.0 \text{ kW}$      $t_p = 6.0 \mu\text{SEC}$      $f_p = 1.0 \text{ kHz}$

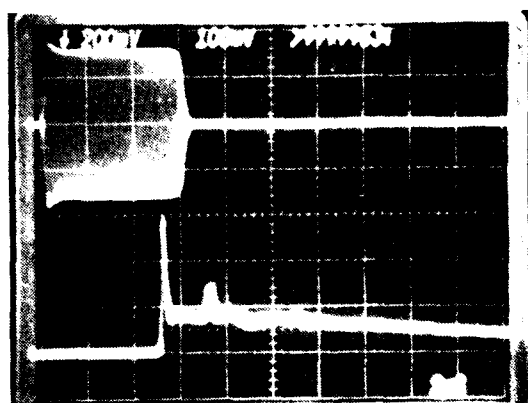
$R = 0.85$      $P = 125 \text{ TORR}$      $P_p \sim 460\text{W}$



MIX 84% (8:1:1) + 16%  $X_e$

$P_{\text{ch}} = 2.0 \text{ kW}$      $t_p = 3.0 \mu\text{SEC}$      $f_p = 1.0 \text{ kHz}$

$R = 0.85$      $P = 125 \text{ TORR}$      $P_p \sim 190\text{W}$

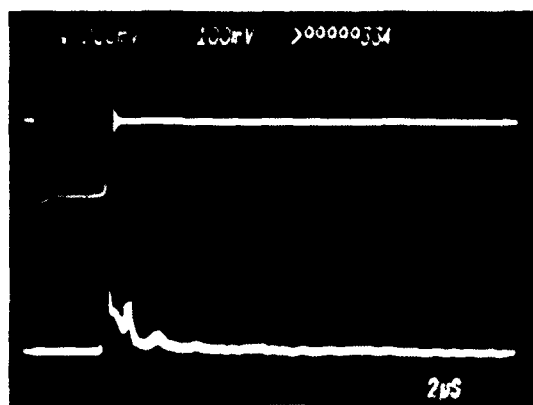


MIX 84% (8:1:1) + 16%  $X_e$

$P_{\text{ch}} = 2.0 \text{ kW}$      $t_p = 6.0 \mu\text{SEC}$      $f_p = 1.0 \text{ kHz}$

$R = 0.85$      $P = 125 \text{ TORR}$      $P_p \sim 140\text{W}$

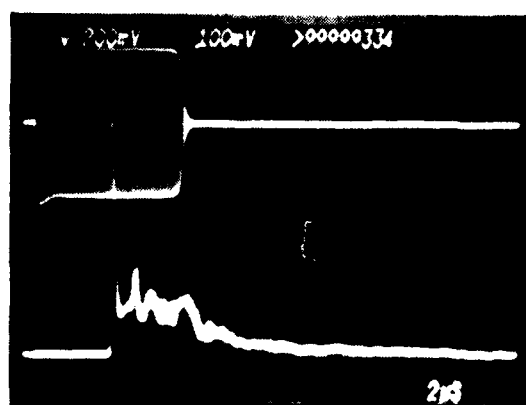
Figure 15. Typical laser power output data for 3:1:1 and 8:1:1 mixes with  $X_e$ .



MIX: 86.3% (3.0.1) + 12.8%  $X_e$  + 0.9%  $H_2O$

$P_{ch}$  2.0 kW  $\tau_p$  3.0  $\mu$ SEC  $f_p$  1.0 kHz

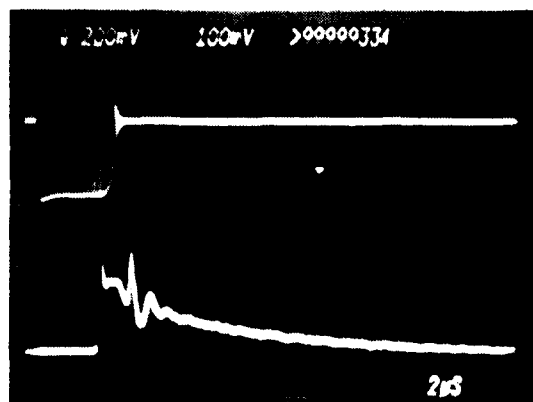
R = 0.85 P = 125 TORR  $P_p \sim 470W$



MIX: 86.3% (3.0.1) + 12.8%  $X_e$  + 0.9%  $H_2O$

$P_{ch}$  2.0 kW  $\tau_p$  6.0  $\mu$ SEC  $f_p$  1.0 kHz

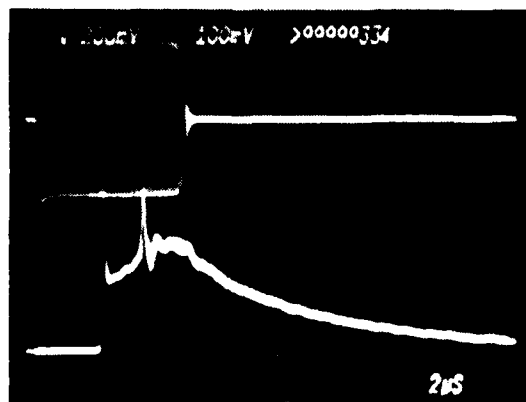
R = 0.85 P = 125 TORR  $P_p \sim 510W$



MIX: 80% (3.0.1) + 12.8%  $X_e$  + 6.4%  $N_2$  + 0.8%  $H_2O$

$P_{ch}$  2.0 kW  $\tau_p$  3.0  $\mu$ SEC  $f_p$  1.0 kHz

R = 0.85 P = 125 TORR  $P_p \sim 600W$



MIX: 80% (3.0.1) + 12.8%  $X_e$  + 6.4%  $N_2$  + 0.8%  $H_2O$

$P_{ch}$  2.0 kW  $\tau_p$  6.0  $\mu$ SEC  $f_p$  1.0 kHz

R = 0.85 P = 125 TORR  $P_p \sim 610W$

Figure 16. Typical laser power output data for (3.0.1) plus  $H_2O$  and  $X_e$  with and without  $N_2$

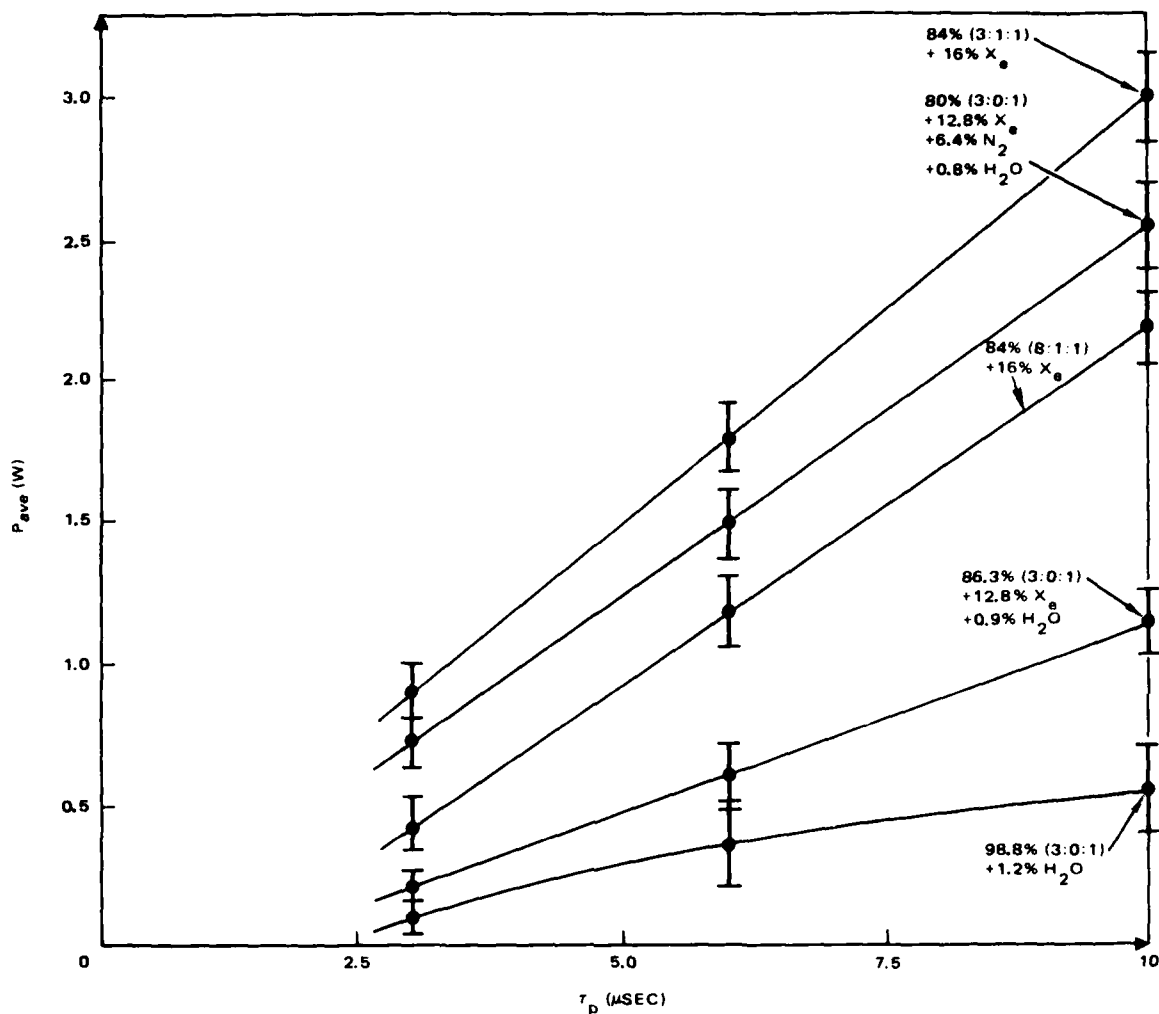


Figure 17.  $P_{ave}$  versus  $\tau_p$  for various gas mixes at  $P = 125$  Torr,  $f_p = 1.0$  kHz, and  $P_{th} = 2.0$  kW.

Figure 18 is a graph of  $P_{ave}$  versus  $X_e$  content for the 3:0:1 plus 1%  $H_2O$  gas mix. Note that the peak in power occurs for 10%  $X_e$  and that additional  $X_e$  does not appreciably increase  $P_{ave}$ . This effect was observed with the other mixes where a 10%  $X_e$  content also produced a near maximum in  $P_{ave}$ .

Figures 19 and 20 are graphs of  $P_p$  and the pulse energy,  $E_p$ , versus  $f_p$  respectively for the 86.3% (3:0:1) + 12.8%  $X_e$  + 0.9%  $H_2O$  gas mix. Note the power roll-off at approximately 3.0 kHz. This roll-off was also typical of the other gas mixes.

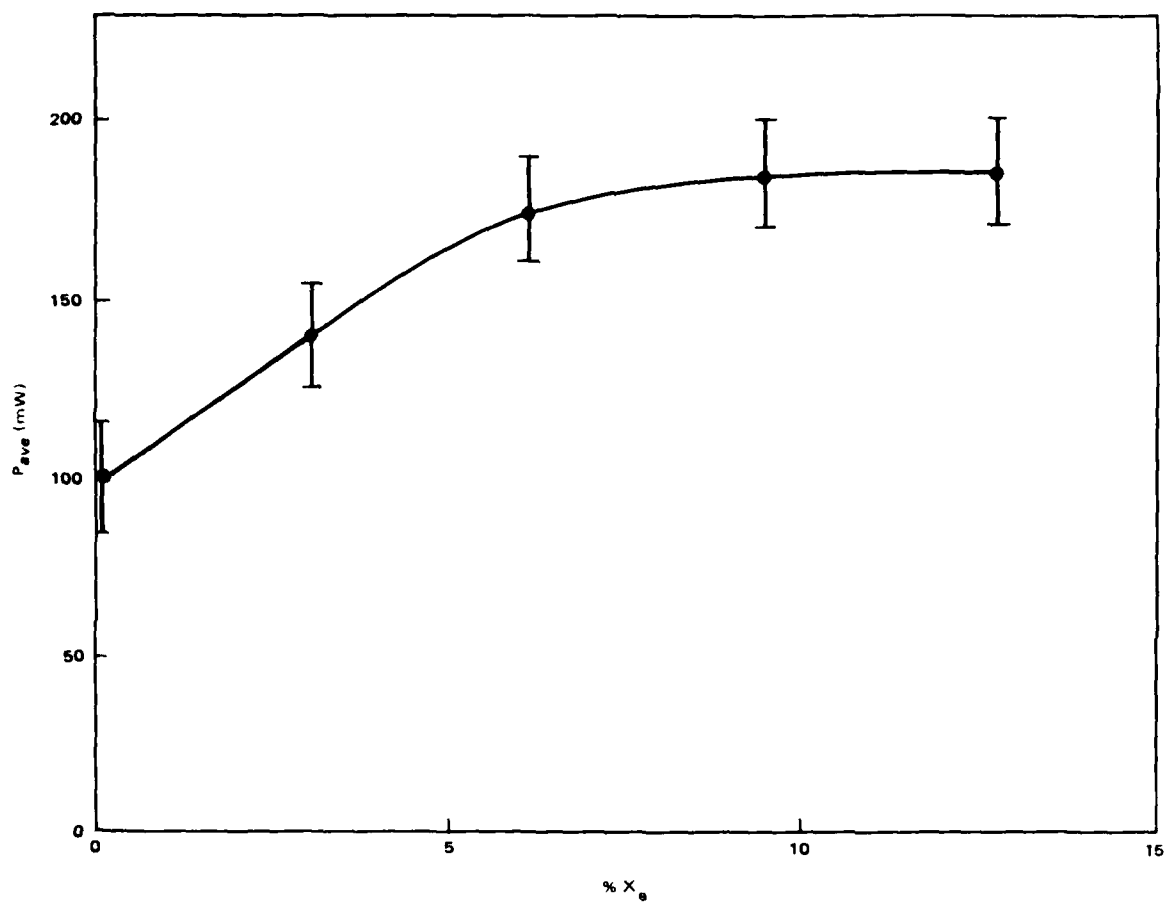


Figure 18.  $P_{ave}$  versus  $X_e$  content for (3:0:1) + 1.0%  $H_2O$  mix at  $P = 125$  Torr,  $\tau_p = 3.0 \mu\text{sec}$ , and  $P_{fh} = 2.0$  kW.

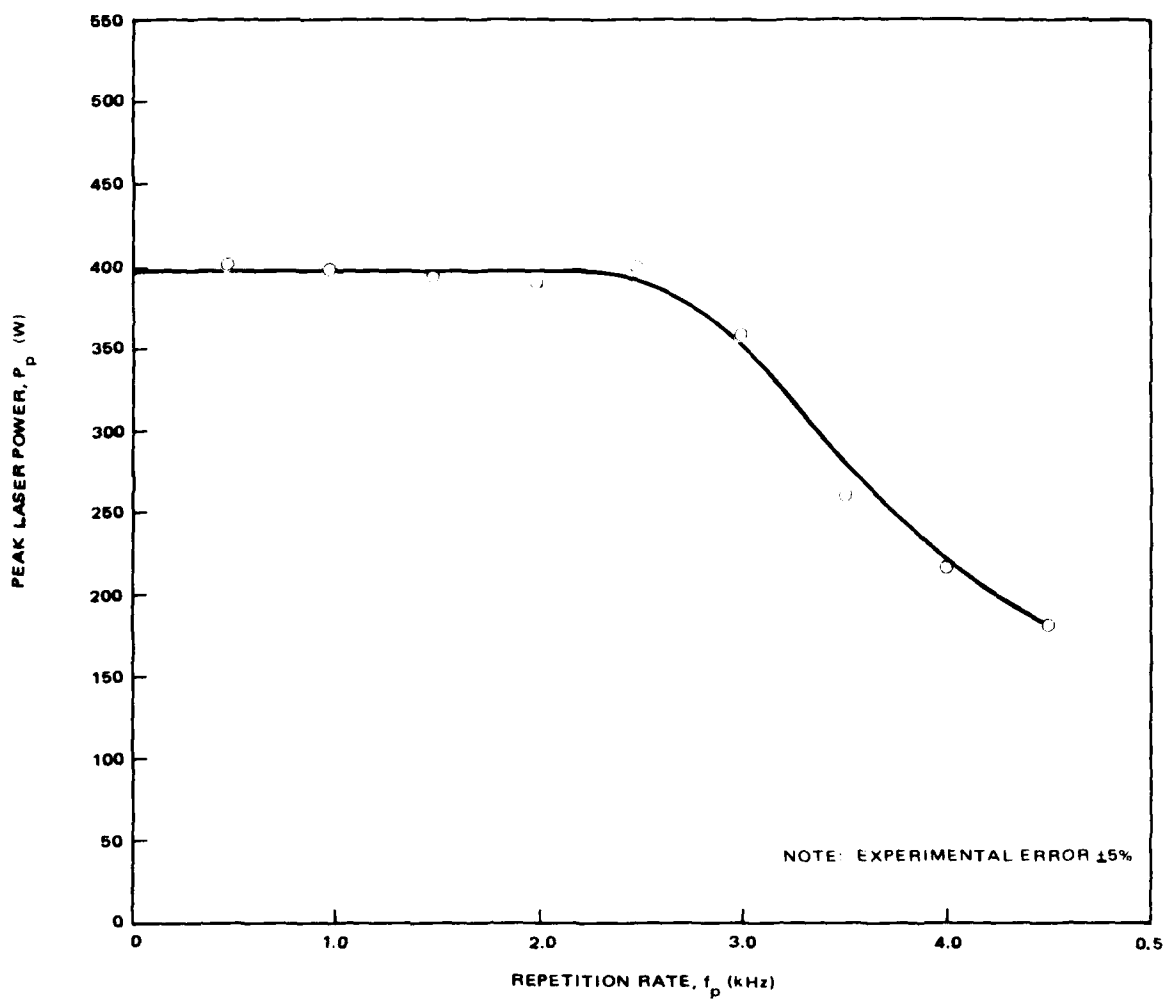


Figure 19.  $P_p$  versus  $f_p$  for 86.3% (3:0:1) + 12.8%  $X_e$  + 0.9%  $H_2O$  mix at  $P = 125$  Torr,  $\tau_p = 3.0 \mu\text{sec}$ , and  $P_{lh} = 2.0$  kW.

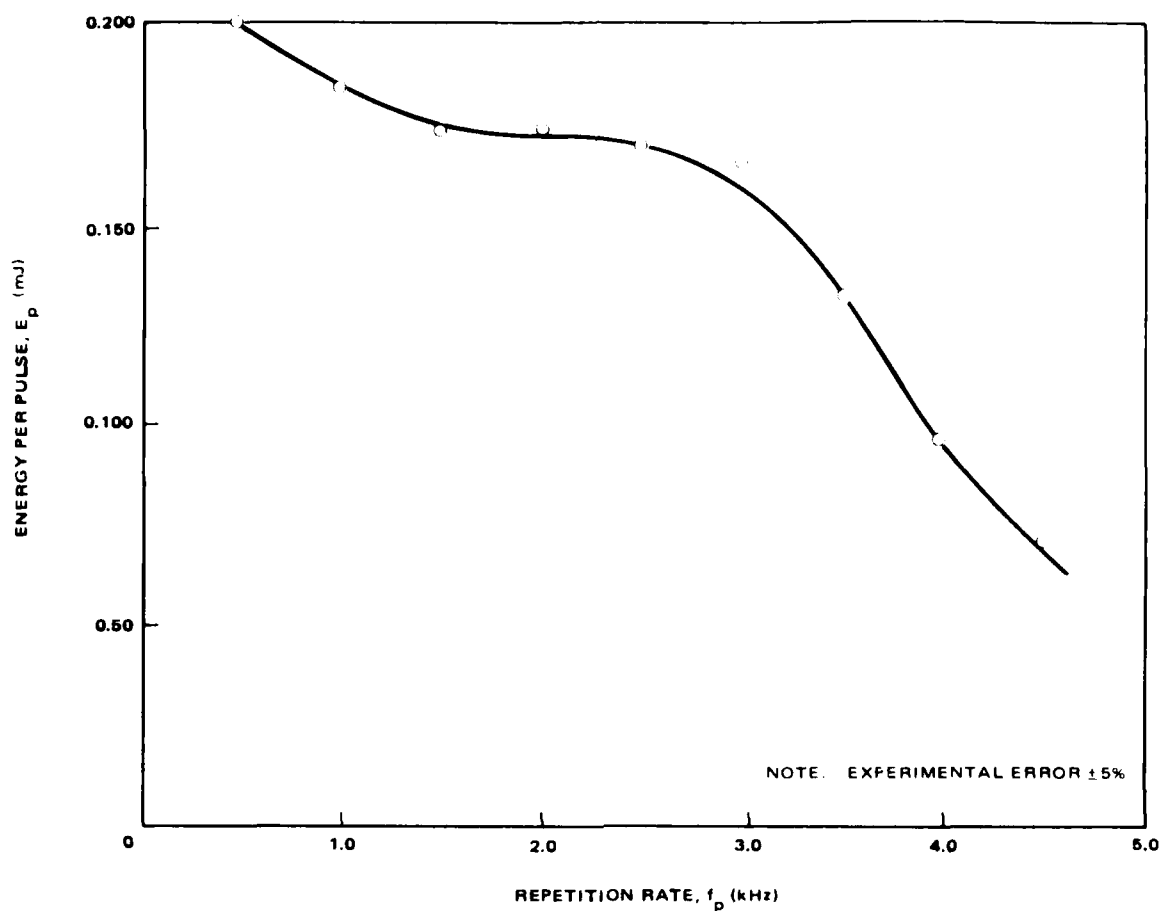


Figure 20.  $E_p$  versus  $f_p$  for 86.3% (3:0:1) + 12.8%  $X_e$  + 0.9%  $H_2O$  at  $P = 125$  Torr,  $\tau_p = 3.0 \mu\text{sec}$  and  $P_{th} = 2.0$  kW.

Figure 21 is a graph of the laser efficiency,  $\eta_l$ , (defined versus  $P_{ave}$  divided by the average rf input power delivered to the laser head) versus  $\tau_p$  for the four gas mixes tested. Note that the efficiency for the 84% (3:1:1) + 16%  $X_e$  is nearly constant with  $\tau_p$  in the 3 to 10  $\mu\text{sec}$  range and that this mix also had the highest overall efficiency at any  $\tau_p$  in this range when compared to the other mixes.

The actual output line of the laser was not monitored during these experiments. Previous data had indicated that the device preferred the 10.2  $\mu$  R band transitions to the 10.6  $\mu$  P band transitions. Since no line selecting elements were used in the experiments, the actual laser output frequency for these experiments occurred in the 10.2  $\mu$  band, R(16) through R(22) region.

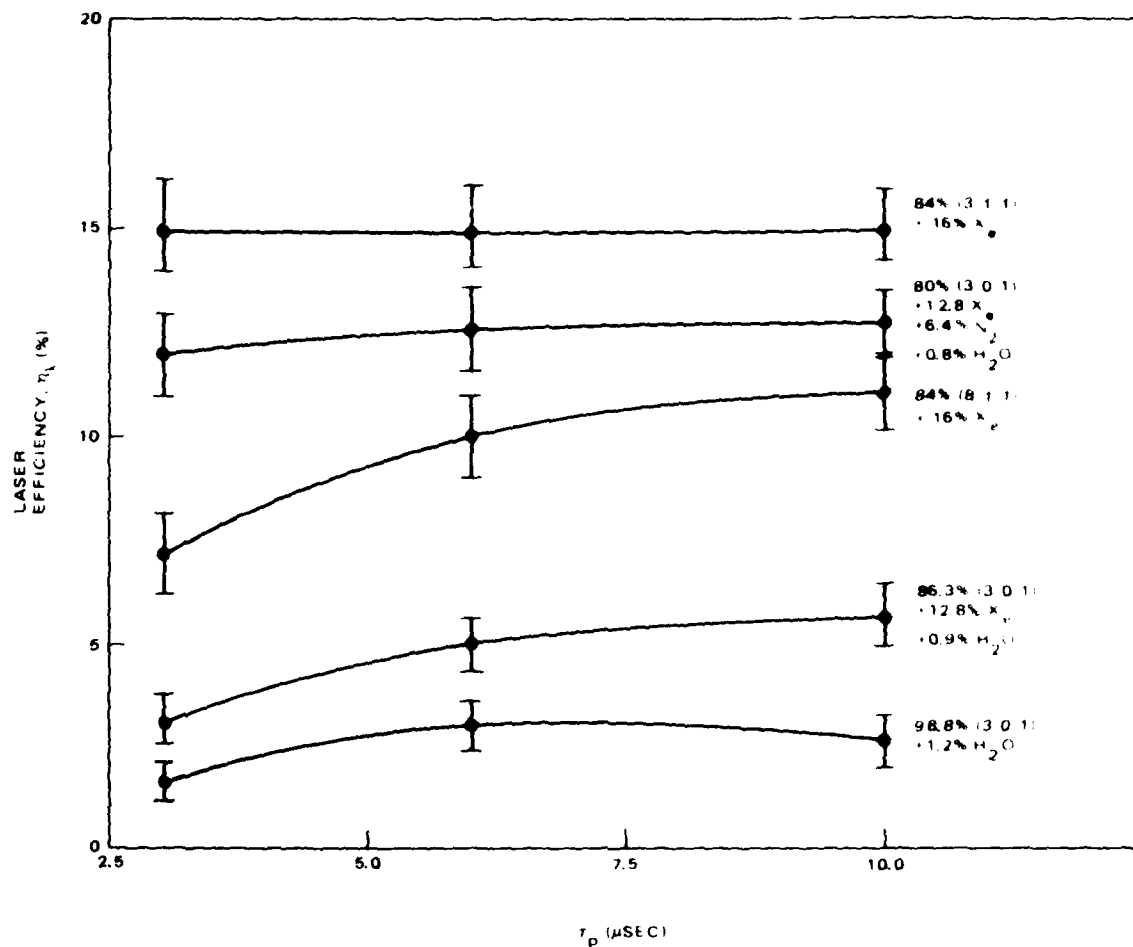


Figure 21.  $\eta_L$  versus  $\tau_p$  for various gas mixes at  $P = 125$  Torr,  $f_p = 1.0$  kHz, and  $P_{th} = 2.0$  kW.

It is also noteworthy that the pulsed rf laser with a heterogeneous waveguide bore (aluminum and ceramic walls) has self-polarized laser output without a Brewster window. The polarization was parallel to the electrode surface in both the sealed and flowing gas power output experiments.

The data obtained for the Phase 2 sealed experiments was excellent and self-consistent. This data is not easily correlated to the Phase 1 flowing data shown in Appendix A due to the difference in resonators and gas mixes. The flowing gas data does indicate that repetition rates of over 20 kHz can be obtained but the sealed data for sealed operation indicates that for this particular laser, 3 to 4 kHz is near the practical limit for sealed operation. Improved designs in the future will no doubt increase the operable repetition rate.

## SEALED LIFE TEST DATA

Sealed life test data was obtained with the pulsed rf laser used in the parametric studies experiments. The laser was operated with an internal flat-flat resonator with mirror reflectivities of 0.95 and 0.90 at 10.6  $\mu\text{m}$ . The 300 cc laser ballast volume was initially filled to a total pressure of 120 Torr with a mixture of 62.5 percent He, 20.8 percent  $\text{CO}_2$ , 16.7 percent  $\text{Xe}$ , 0.83 percent  $\text{H}_2$ , and 0.41 percent  $\text{O}_2$ . The laser was then run for 318 hours at a 1.0 kHz repetition rate (1.1 billion pulses) with 2.1 kW input power and with a 2.2  $\mu\text{sec}$  rf input pulsewidth. The laser initially had been thoroughly cleaned but had not been baked out nor had the laser been prerun to partially passivate the aluminum internal structure. The laser power output (both average and peak) was monitored during the experiment. The laser optics at one end were occasionally adjusted to maintain P(1r) operation on the lowest order mode as the thermal expansion of the aluminum, and thus the laser mode would vary with ambient temperature due to changes in the resonator length.

No other adjustments were made during the experiment.

## Results

The peak laser output power of 300W did not vary significantly during the life test but the initial average power of 110 mW did degrade slightly to 105 mW at the end of the experiment. This was attributed to a slight decrease in the power in the tail of the gain-switched spike.

The gas mix was analyzed after the life test with a Varian Aspect RM600 mass spectrometer to determine the final gas composition. By carefully comparing the life test mix against the initial mix and with synthesized mixes containing CO and also by taking data at high and low accelerating voltages, the following conclusions were reached:

1. The final  $\text{CO}_2/\text{CO}$  molecular ratio in the life test mix was about 1:1 (~17 percent dissociation of  $\text{CO}_2$ ).
2. No 14 amu peaks were observed at high accelerating voltages indicating no air leaks into the laser mix during the experiment.
3. No residual molecular or atomic oxygen was observed in the life test mix indicating that oxidation of the internal aluminum structure had occurred with oxygen supplied from the dissociated  $\text{CO}_2$ .

Since no processing of the laser was performed prior to the life test, the amount of oxidation that occurred during the experiment is not surprising. The total number of pulses that occurred during the life test (1.1 billion) is significant and indicates that the rf discharge is indeed a fairly benign method of obtaining optical gain by means of a non-preionized discharge.

Future experiments are needed to determine passivation techniques to further minimize the  $\text{CO}_2$  dissociation.

#### AMPLITUDE AND FREQUENCY STABILITY DATA

Data was obtained with regard to amplitude and frequency stability on the sealed pulsed rf laser.

Figure 22 is a photo of approximately 250 overlapped oscilloscope traces of the gain-switches laser output which is typical of the amplitude stability observed with this laser. Note that the 320 W peak laser power was stable to within a few percent during the 1/4 second photo with  $f_p = 1.0 \text{ kHz}$  as measured with a calibrated 20 MHz pyroelectric detector (1.0 mV/watt).

Amplitude stability normally implies frequency stability when dealing with pulsed lasers. Figure 23 is the actual heterodyne signal of the pulsed rf  $\text{CO}_2$  laser and a frequency stable (50 kHz/msec) cw Sylvania  $\text{CO}_2$  laser

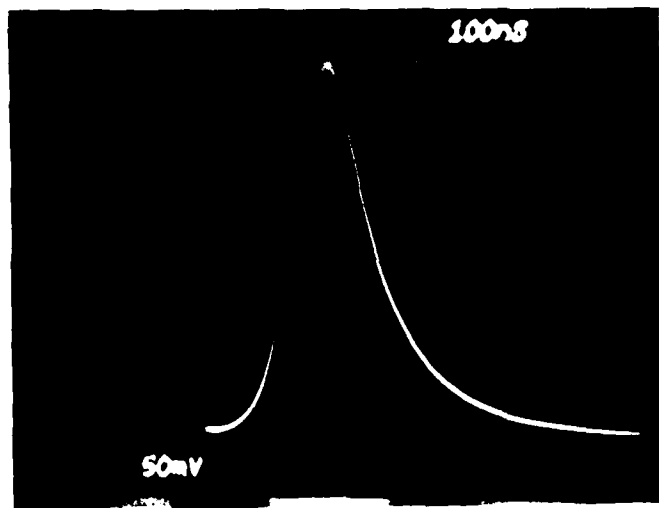


Figure 22. Typical multipulse laser output with  $P_{ch} = 2.0 \text{ kW}$ ,  $f_p = 1.0 \text{ kHz}$ , and  $\tau_p = 3.0 \mu\text{sec}$  (1/4 second photo).

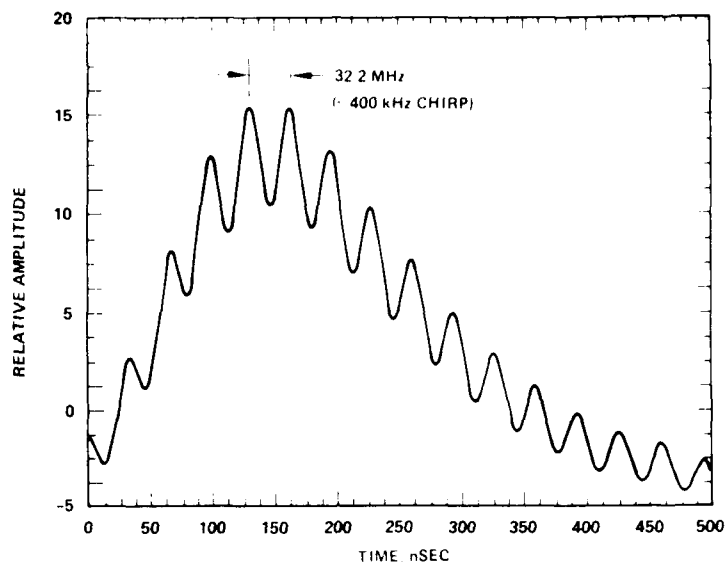


Figure 23. Typical single pulse heterodyne signal of the pulsed rf laser, and a cw reference with  $P_{ch} \cong 2.0$  kW,  $f_p = 2.0$  kHz, and  $\tau_p = 3.0$   $\mu$ sec.

both tuned to line center of the  $10.6 \mu$  P(20) transition. The pulsed heterodyne signal was analyzed with a transient digitizer set to 4 nSEC resolution. Over the FWHM of the pulse, no chirp was observed. Some chirp was noted in the tail of the pulse. Pulse-to-pulse stability as determined visually on the oscilloscope appeared to be better than 1%. Mechanical shock applied to the laser via a small plastic hammer did not appear to change the heterodyne frequency thus indicating mechanical insensitivity.

This data indicates that the pulsed rf laser will be useful in small pulsed coherent detection schemes where small size, moderate power levels, and mechanical noise insensitivity are required.

## CONCLUSIONS AND OBSERVATIONS

The Pulsed RF Waveguide Studies Program has been successfully completed. Both flowing and sealed data has been obtained and hardware has been built under this effort. Several observations can be made at this time:

1. Sealed pulsed laser output efficiencies of up to 15 percent have been experimentally obtained with certain gas mixes. This efficiency was calculated by dividing the average laser output power by the average rf power delivered to the laser head.
2. Peak small signal gains of up to 2.7 percent/cm (flowing) and 2.3 percent/cm (sealed) have been realized.
3. Operation at repetition rates of over 20 kHz have been obtained with flowing gas and over 3.0 kHz sealed.
4. Peak gain-switched power outputs of over 600 W have been observed.
5. Continuous operation of over 1.1 billion shots has been performed on a sealed laser with minimal power degradation during the experiment.
6. Inherent amplitude and frequency stabilities in this device indicate that pulsed coherent detection can easily be performed.

The pulsed rf waveguide laser needs further development in several areas. One area is the miniaturization of the power supply for tactical considerations. Secondly, increased output power in the gain switched pulse is needed for improved range in coherent tactical systems. Thirdly, the decrease in sealed off power output with repetition rate must be further investigated so that higher average powers and data rates can be achieved which are important from a tactical systems point of view. Also miniaturized sealed life test devices must be built and tested to determine ultimate temporal performance both on the shelf and in operation.

The pulsed rf wavelength  $\text{CO}_2$  laser will be most useful from a tactical point of view in pulsed coherent detection schemes. Although these systems are not currently in major use in the military, future systems may require them based on various tactical considerations.

## ACKNOWLEDGEMENTS

Special thanks is given to Glenn Griffith and Robert Washburn for their assistance in designing the monitoring and discharge matching electronics and for their overall technical assistance. Technical electronics assistance by Max Miller and Mike Davison was also appreciated.

Apparatus fabrication and assembly was performed on internal Hughes funding by Milt Blake, Robert Eldridge, Sho Tsubakahara, Jim Jacobson, and Robert Voreis, to whom I give special thanks.

## REFERENCES

1. Sutter, L., "Pulsed RF Waveguide Studies Program, Phase 1 Report," Report No. DELNV-TR-78-2450-1, August 1979.
2. Ramo, Whinnery, and Van Duzer, Fields and Waves in Communication Electronics, Wiley and Sons, New York, 1965.
3. Sutter, L., "Analysis of Continuous Electron Gun Pre-Ionized Electric Laser Discharges," PhD dissertation at UCLA, 1977.
4. Lowke et al, J. App. Phys., 44, 4664 (1973).
5. Yariv, A., Introduction to Optical Electronics, Holt, Reinhart, and Winsten, 1971.
6. Abrams, R.L., J. Quan. Elec., QE-8, 838 (1972).
7. Marcatili, E.A., Bell Sys. Tech. J., 2071 (September 1969).
8. Marcatili, E.A., and Schmeltzer, R.A., Bell Sys. Tech. J., 1783 (July 1964).

## APPENDIX

This appendix contains a synopsis of the Phase 1 flowing gas experiments and results. Some corrections to the Phase 1 Report No. DELNV-TR-78-2450-1 have been included. The laser used in the flowing gas experiments differed from the one used in the sealed experiments of Phase 2 in that the former device employed BeO walls and a 2.0 mm bore while the latter device employed alumina walls and a 2.5 mm bore. Also the laser extraction measurements with the flowing gas device used external resonator optics whereas the sealed device experiments used a lower loss internal resonator. Thus a direct comparison of the two data sets is not easily performed and no effort will be made here to do this comparison other than in general terms.

### FLOWING GAS EXPERIMENTAL RESULTS

Small signal gain and extracted output power data under flowing gas conditions was obtained for the pulsed rf waveguide laser. This data was obtained by parametrically varying the experimental variables such as discharge pulsewidth, pulse repetition rate, input power, gas mix, gas pressure, and gas flow rate. To minimize the amount of data, the gas pressure was set to that value which produced the largest output power spike obtained for the corresponding laser extraction experiments. Also the gas flow rate was set to a maximum for the given gas pressure as limited by the gas plumbing flow constrictions. The power input was essentially fixed for the gas mixes containing  $N_2$  to the highest power output delivered from the power supply at the 10 kHz repetition rate so that the power output results at various repetition rates could be compared at constant input power. The power input was increased for the gas mixes without  $N_2$  due to the decreased pumping efficiency for these mixes. (See Figure A1.)

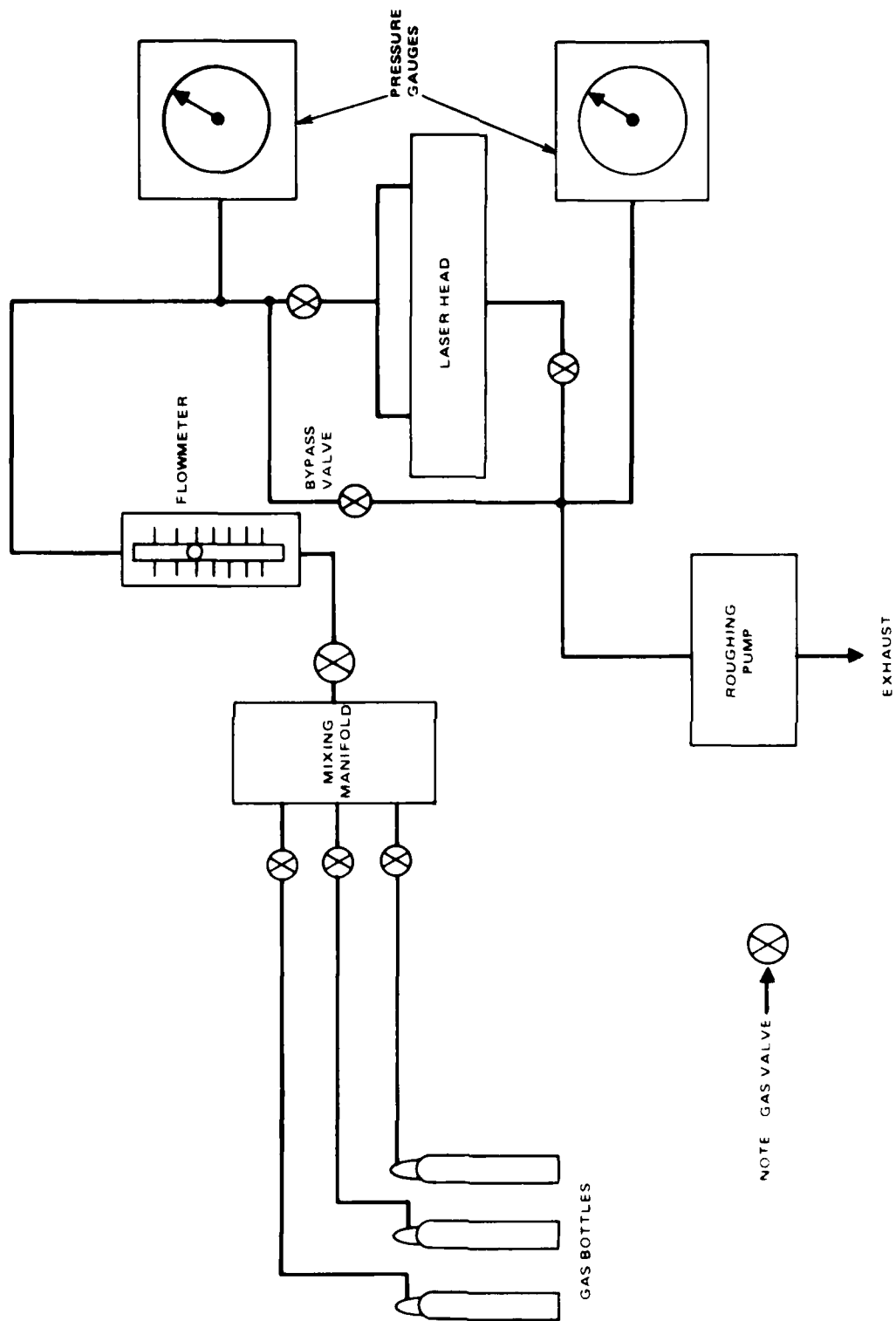


Figure A1. Gas plumbing layout for flowing gas experiments.

## FLOWING GAS GAIN DATA

### Experimental Setup and Discussion

Figure A2 illustrates the experimental arrangement for the small signal gain experiments. The attenuated 5 mW beam from a Sylvania  $\text{CO}_2$  stabilized laser was tuned to the line center of the  $10.6\mu$  P20 transition. The beam then reflected from a mirror and was focused by an  $f = 7.5$  cm ZnSe lens into the waveguide bore. The beam passing out of the waveguide bore was imaged on the HgCdTe 10 MHz detector by placing a ZnSe lens of  $f = 7.5$  cm at twice this distance from the laser bore and the detector thereby eliminating steering effects of the pulsed heated gas. A manually operated blocking screen was placed directly in front of pulsed device so that a zero level reading could be obtained for the dc coupled detector by blocking the probe beam. The detector was connected by a 50 ohm line to a high impedance, dual trace, band-limited 200 MHz scope in parallel to a 51 ohm termination. The other channel of the scope was used to record the attenuated forward voltage signal.

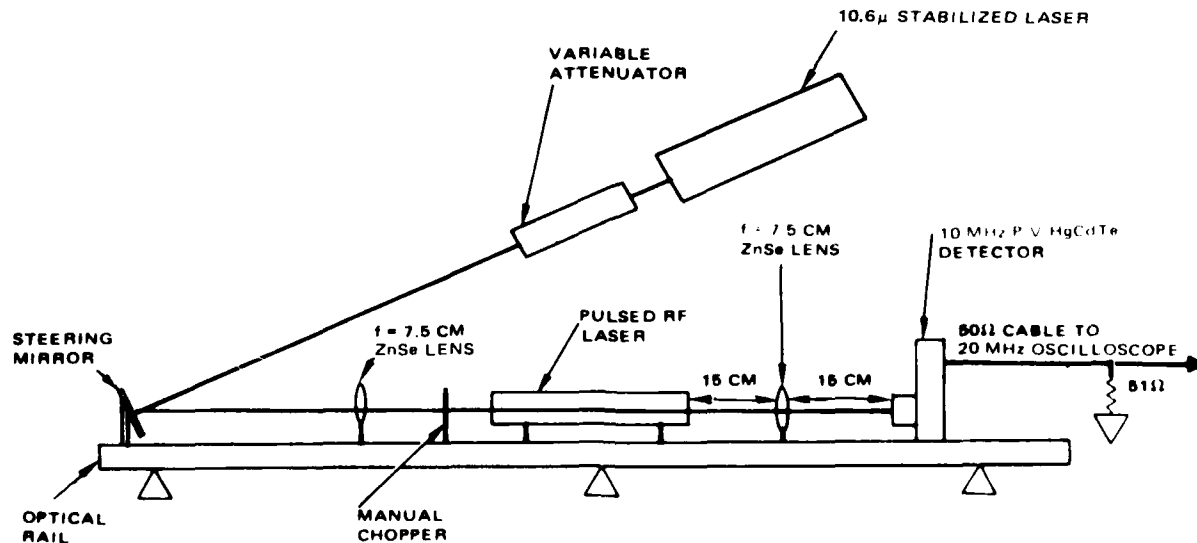


Figure A2. Flowing gas small signal gain experimental apparatus.

## Results

Data was obtained on 8:1:1, 3:1:1, and 3:0:1 (He:N<sub>2</sub>:CO<sub>2</sub>) gas mixes. Only small signal gain was measured and no saturated data was taken. The data will be presented in tabular form using the following variables to describe the measurement data:

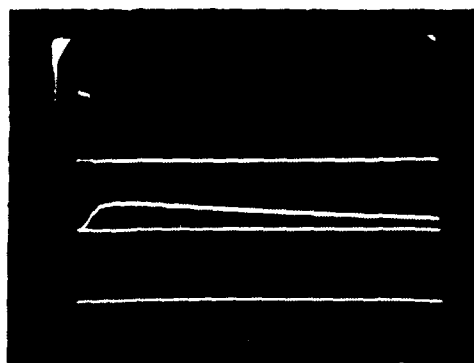
- $P_{lh}$  - average pulse power into the lower head in kW
- $\tau_p$  - pulsewidth of the forward power pulse in sec
- $f_p$  - the pulsewidth repetition rate in kHz
- $g_p$  - the peak measured small signal gain in cm<sup>-1</sup>
- $\tau_d$  - the characteristic decay time of the gain after reaching  $g_p$  in  $\mu$ sec

This data is presented in Table A1. Figures A3 and A4 illustrate the actual data taken for various experimental conditions. The small signal gain versus time is illustrated in these figures and is determined by the lower three traces of each photo. The upper of the three traces is the detector signal with input power pulse to the pulsed laser. The next lower line is the detector signal without power pulse to the pulsed laser. The lowest line is the zero level of the detector. Thus these three traces determine the small signal gain of the laser medium versus time. The uppermost trace is the attenuated rectified envelope of the forward voltage pulse.

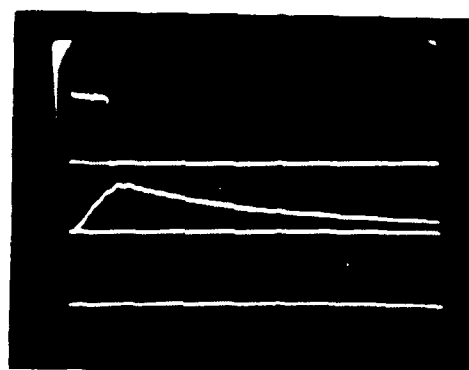
There are several interesting aspects to this data. We note that of the three mixes measured, the 3:1:1 mix had the highest  $g_p$  followed by 8:1:1 and 3:0:1 respectively. The value of  $g_p$  in nearly all the cases peaks after the power pulse as would be expected since at the end of the pulse the pumping of the lower laser level ceases thus increasing the inversion just after the pulse due to the rapid decay of this level which increases the gain. Also note that the 3:0:1 mix has the most rapid decay of the gain as compared to the other mixes. This is mostly due to the high relative CO<sub>2</sub> content as CO<sub>2</sub> molecules are more likely to deactivate excited CO<sub>2</sub> molecules in a collision than are He and N<sub>2</sub>. The highest small signal gain measured was 2.7 percent/cm for the 3:1:1 mix with  $f_p = 1.0$  kHz,  $\tau_p = 10.0$   $\mu$ sec, and  $P_{lh} = 2.0$  kW. This does not mean that the 3:1:1 mix is the absolute best in terms of small signal gain when compared against all other He:N<sub>2</sub>:CO<sub>2</sub> mixes. This mix was chosen as a reference to the 8:1:1 mix of which there is some published laser

TABLE A1. FLOWING GAS SMALL SIGNAL GAIN DATA

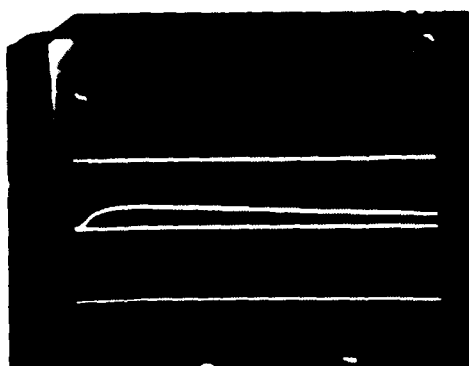
Gas Mix	$P_{th}$ (kW)	$\tau_p$ ( $\mu$ sec)	$f_p$ (kHz)	P (Torr)	$\dot{n}$ (millimoles/sec)	$\tau_d$ ( $\mu$ sec)	$g_p$ (%/cm)
3:1:1	2.0	3.0	1.0	100	2.4	80	1.8
3:1:1	2.0	6.0	1.0	100	2.4	70	2.5
3:1:1	2.0	10.0	1.0	100	2.4	60	2.7
3:1:1	1.6	3.0	10.0	100	2.4	85	0.9
3:1:1	1.6	9.5	3.0	100	2.4	80	2.5
8:1:1	2.0	3.0	1.0	100	2.4	160	1.5
8:1:1	2.0	6.0	1.0	100	2.4	150	2.2
8:1:1	2.0	10.0	1.0	100	2.4	130	2.3
8:1:1	1.6	3.0	10.0	100	2.4	130	1.4
8:1:1	1.7	9.5	3.0	100	2.4	130	2.2
3:0:1	2.5	3.0	1.0	180	4.5	40	1.1
3:0:1	2.5	6.0	1.0	180	4.5	30	1.6
3:0:1	2.5	10.0	1.0	180	4.5	30	1.8
3:0:1	2.5	3.0	3.0	180	4.5	30	1.0
3:0:1	1.6	3.0	10.0	180	4.5	—	0.7
3:0:1	2.5	3.0	3.0	100	2.4	50	1.2
3:0:1	2.5	10.0	1.0	100	2.4	30	2.1



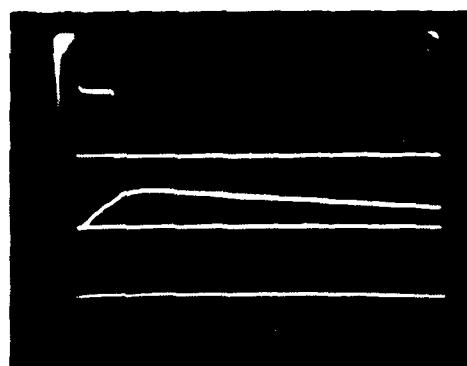
3:1:1 MIX  $\tau_p = 10 \mu\text{SEC}$   $f_p = 1.0 \text{ KHZ}$   
 $P_{\text{IN}} = 2.0 \text{ KW}$   $\tau_d = 80 \mu\text{SEC}$   $p_p = 0.018 \text{ CM}$   
 100 TORR



3:1:1 MIX  $\tau_p = 10 \mu\text{SEC}$   $f_p = 1.0 \text{ KHZ}$   
 $P_{\text{IN}} = 2.0 \text{ KW}$   $\tau_d = 80 \mu\text{SEC}$   $p_p = 0.02 \text{ CM}$   
 100 TORR

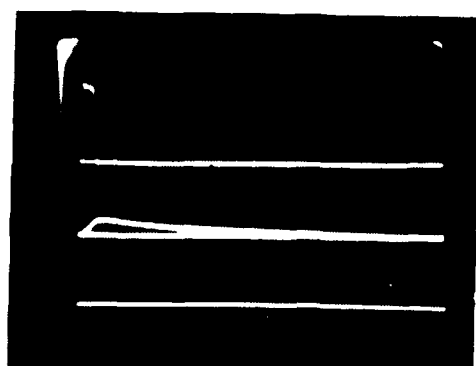


8:1:1 MIX  $\tau_p = 10 \mu\text{SEC}$   $f_p = 1.0 \text{ KHZ}$   
 $P_{\text{IN}} = 2.0 \text{ KW}$   $\tau_d = 160 \mu\text{SEC}$   $p_p = 0.015 \text{ CM}$   
 100 TORR

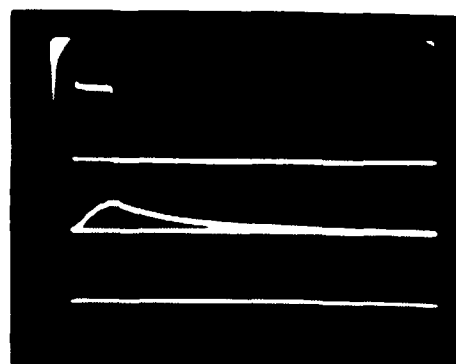


8:1:1 MIX  $\tau_p = 10 \mu\text{SEC}$   $f_p = 1.0 \text{ KHZ}$   
 $P_{\text{IN}} = 2.0 \text{ KW}$   $\tau_d = 160 \mu\text{SEC}$   $p_p = 0.02 \text{ CM}$   
 100 TORR

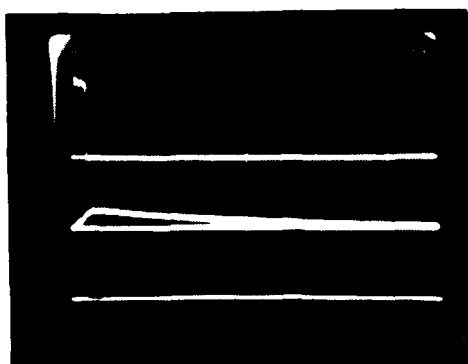
Figure A3. Typical small signal gain data with flowing gas for 3:1:1 and 8:1:1 mixes at 100 torr gas pressure. (Note: All photos  $10 \mu\text{sec/div}$  time scale.)



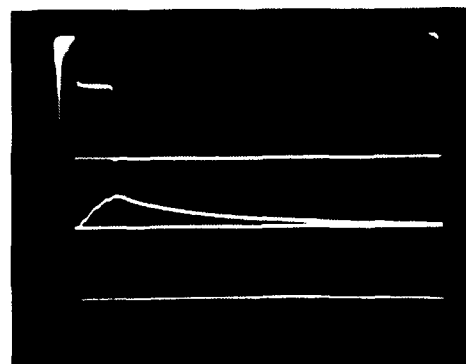
$f_{in} = 1.0 \text{ MHz}$      $f_{out} = 10 \text{ kHz}$   
 $P_{in} = 2.5 \text{ kW}$      $P_{out} = 40 \text{ mW}$      $g_p = 0.013 \text{ M}$   
 $\lambda = 100 \text{ cm}$



$f_{in} = 1.0 \text{ MHz}$      $f_{out} = 10 \text{ kHz}$   
 $P_{in} = 2.5 \text{ kW}$      $P_{out} = 40 \text{ mW}$      $g_p = 0.013 \text{ M}$   
 $\lambda = 100 \text{ cm}$



$f_{in} = 1.0 \text{ MHz}$      $f_{out} = 10 \text{ kHz}$   
 $P_{in} = 2.5 \text{ kW}$      $P_{out} = 40 \text{ mW}$      $g_p = 0.013 \text{ M}$   
 $\lambda = 100 \text{ cm}$



$f_{in} = 1.0 \text{ MHz}$      $f_{out} = 10 \text{ kHz}$   
 $P_{in} = 2.5 \text{ kW}$      $P_{out} = 40 \text{ mW}$      $g_p = 0.013 \text{ M}$   
 $\lambda = 100 \text{ cm}$

Figure A4. Typical small signal gain data with flowing gas for 3 0 1 mix. (Note: All photos 10  $\mu\text{sec/div}$  time scale.)

kinetics data. The 3:1:1 mix has twice the  $N_2$  and  $CO_2$  content of 8:1:1 and thus makes an interesting mix for comparative reasons.

## FLOWING GAS POWER OUTPUT DATA

### Experimental Setup and Discussion

Figure A5 illustrates the experimental arrangement for the power output measurements. The pulsed rf laser was operated with external optics mounted to a thermally and mechanically stable rail. AR windows at 10.6  $\mu$  were mounted to the ends of the laser shell and formed the gas seals. The gas was flowed as in the small signal gain experiments by flowing the gas through both ends of the bore and out a hole in the center of the grounded discharge electrode. The average laser output power was measured with a Coherent Radiation model No. 210 power meter. The actual pulse shape of the output was measured by observing the residual scattered radiation from the power meter detector head with a 75 MHz HgCdTe detector. This detector has a 10 MHz bandwidth without the bias box (as was used in the small signal gain experiments). The detector was terminated into a dual trace high impedance scope in parallel with a 51 ohm termination. The scope was band-limited to 20 MHz to prevent rf noise signals from being displayed on the oscilloscope. The other channel of the scope was used to record the rectified envelope of the forward voltage pulse. The setting of the oscilloscope. The other channel of the scope was used to record the rectified envelope of the forward voltage pulse. The setting of the oscilloscope to the 20 MHz band-limit did not significantly alter the output power trace. The detector was decoupled with a slow (10 Hz) response so that both the initial power spike and long tail in mixtures containing  $N_2$  could be observed undistorted. By measuring the time averaged output power and observing the fast detector trace, the peak output power was determined.

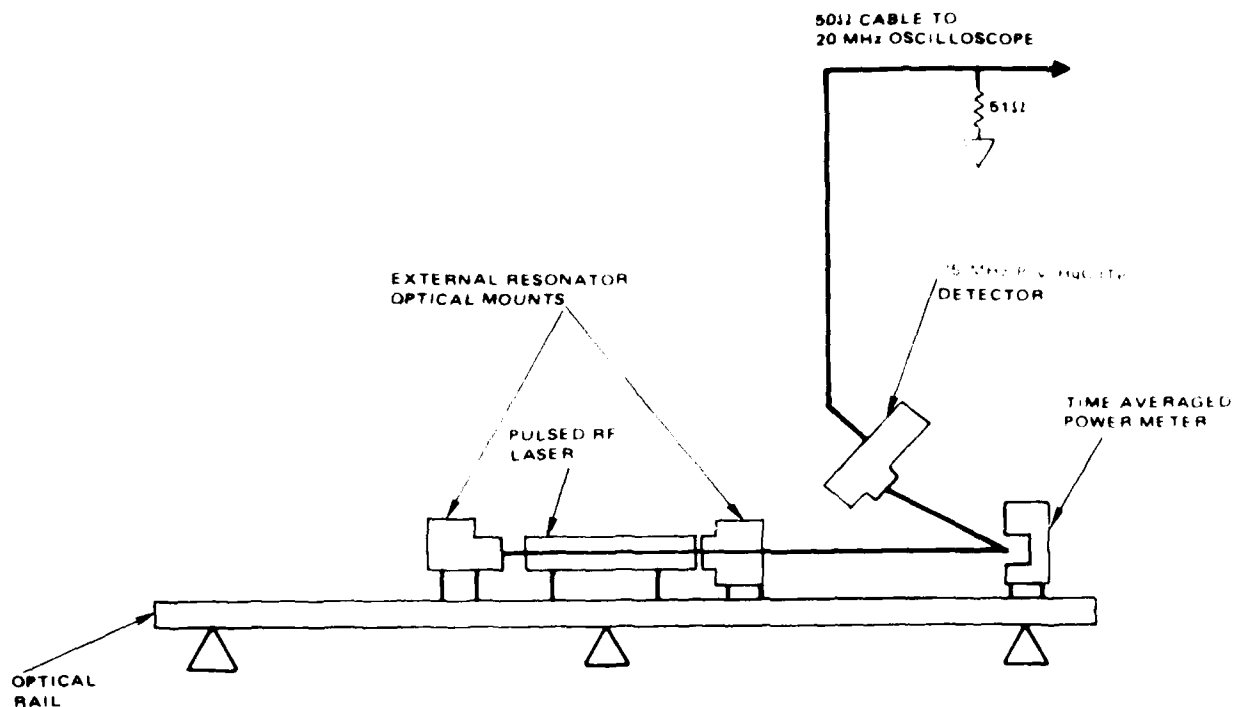


Figure A5. Flowing gas power output experimental apparatus.

### Results

Data was obtained on 8:1:1, 3:1:1, and 3:0:1 (He:N<sub>2</sub>:CO<sub>2</sub>) gas mixes. The data will be presented in tabular form using the same nomenclature as Table A1 with the added measurement variables:

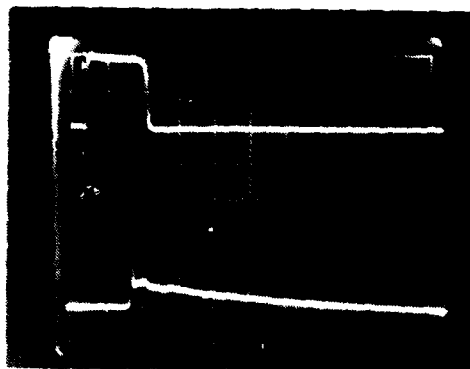
$P_p$  = the peak output power from the laser in watts  
 $P_{ave}$  = the average laser output power in watts

This data is presented in Table A2. Figures A6 and A7 illustrate the actual output data taken for various experimental conditions. The lower trace in each photo is the fast detector trace of the power output while the upper trace represents the attenuated rectified envelope of the forward voltage pulse.

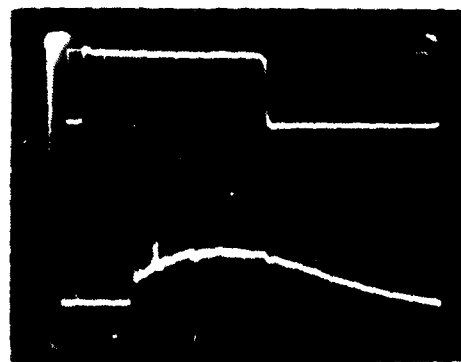
There are some noteworthy aspects to this data. The best average output power from the pulsed laser was obtained with the 3:1:1 mix followed by 8:1:1 and 3:0:1 respectively. The highest peak power output of the laser

TABLE A2. FLOWING GAS POWER OUTPUT DATA

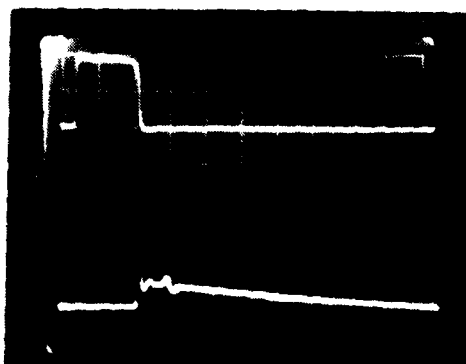
Gas Mix	P <sub>th</sub> (kW)	$\tau_p$ ( $\mu$ sec)	f <sub>p</sub> (kHz)	P Torr	n (millimoles/sec)	R	P <sub>p</sub> (Watts)	P <sub>ave</sub> (Watts)
3:1:1	2.0	3.0	1.0	100	2.4	0.70	~220	0.20
3:1:1	2.0	6.0	1.0	100	2.4	0.70	~200	0.55
3:1:1	2.0	10.0	1.0	100	2.4	0.70	~220	0.70
3:1:1	1.6	3.0	10.0	100	2.4	0.70	~80	0.90
3:1:1	1.8	9.5	3.0	100	2.4	0.70	~130	1.55
3:1:1	2.0	3.0	1.0	100	2.4	0.80	~130	0.20
3:1:1	2.0	6.0	1.0	100	2.4	0.80	~280	0.55
3:1:1	2.0	10.0	1.0	100	2.4	0.80	~240	0.65
3:1:1	1.6	3.0	10.0	100	2.4	0.80	~80	0.70
3:1:1	1.7	9.5	3.0	100	2.4	0.80	~300	1.45
3:1:1	2.0	3.0	1.0	100	2.4	0.90	~160	0.25
3:1:1	2.0	6.0	1.0	100	2.4	0.90	~210	0.55
3:1:1	2.1	10.0	1.0	100	2.4	0.90	~210	0.65
3:1:1	1.6	3.0	10.0	100	2.4	0.90	~100	0.95
3:1:1	1.7	9.5	3.0	100	2.4	0.90	~130	1.55
8:1:1	2.0	3.0	1.0	100	2.4	0.70	~120	0.15
8:1:1	2.0	6.0	1.0	100	2.4	0.70	~130	0.35
8:1:1	2.0	10.0	1.0	100	2.4	0.70	~140	0.60
8:1:1	1.6	3.0	10.0	100	2.4	0.70	~60	0.80
8:1:1	1.7	9.5	3.0	100	2.4	0.70	~170	1.30
8:1:1	2.0	3.0	1.0	100	2.4	0.80	~140	0.15
8:1:1	2.0	6.0	1.0	100	2.4	0.80	~170	0.35
8:1:1	2.0	10.0	1.0	100	2.4	0.80	~190	0.60
8:1:1	1.6	3.0	10.0	100	2.4	0.80	~80	0.85
8:1:1	1.8	9.5	3.0	100	2.4	0.80	~190	1.15
8:1:1	2.0	3.0	1.0	100	2.4	0.90	~140	0.20
8:1:1	2.0	6.0	1.0	100	2.4	0.90	~130	0.40
8:1:1	2.0	10.0	1.0	100	2.4	0.90	~150	0.70
8:1:1	1.7	3.0	10.0	100	2.4	0.90	~80	1.20
8:1:1	1.7	9.5	3.0	100	2.4	0.90	~130	1.45
3:0:1	2.5	3.0	1.0	180	4.5	0.95	~400	0.10
3:0:1	2.5	6.0	1.0	180	4.5	0.95	~310	0.18
3:0:1	2.5	3.0	3.0	180	4.5	0.95	~280	0.20
3:0:1	2.3	3.0	3.0	100	2.4	0.95	~170	0.18



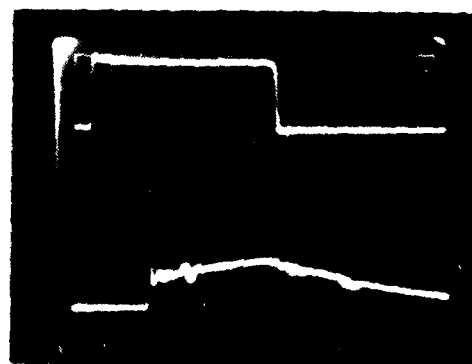
3:1:1 MIX  $f_{mod} = 100 \text{ kHz}$   $P_{out} = 2.0 \text{ kW}$   
 $P_{in} = 140 \text{ W}$   
 $P_{eff} = 0.000$



3:1:1 MIX  $f_{mod} = 100 \text{ kHz}$   $P_{out} = 2.0 \text{ kW}$   
 $P_{in} = 140 \text{ W}$   
 $P_{eff} = 0.000$

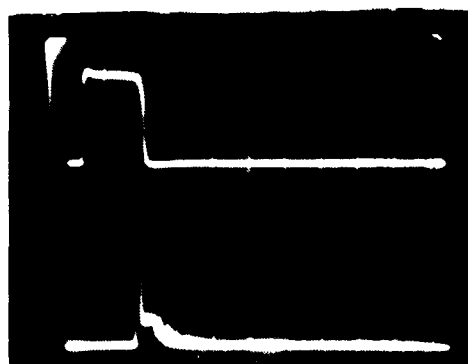


8:1:1 MIX  $f_{mod} = 100 \text{ kHz}$   $P_{out} = 2.0 \text{ kW}$   
 $P_{in} = 140 \text{ W}$   
 $P_{eff} = 0.000$

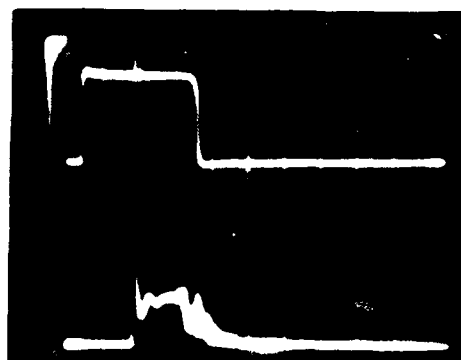


8:1:1 MIX  $f_{mod} = 100 \text{ kHz}$   $P_{out} = 2.0 \text{ kW}$   
 $P_{in} = 140 \text{ W}$   
 $P_{eff} = 0.000$

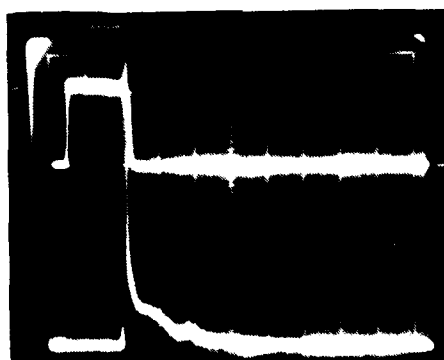
Figure A6. Typical laser output data with flowing gas for 3:1:1 and 8:1:1 gas mixes at 100 torr gas pressure. (Note: All photos 2  $\mu\text{sec/div}$  time scale.)



$10:1 \text{ MIX}$        $t_p = 10 \mu\text{SEC}$        $f_p = 10 \text{ KHZ}$   
 $P_{AV} = 2.5 \text{ KW}$      $P = 150 \text{ TOHR}$      $P_p = 150 \text{ W}$   
 $R = 0.95$



$10:1 \text{ MIX}$        $6.0 \mu\text{SEC}$        $10 \text{ KHZ}$   
 $P_{AV} = 2.5 \text{ KW}$      $P = 150 \text{ TOHR}$      $P_p = 150 \text{ W}$   
 $R = 0.95$



$10:1 \text{ MIX}$        $t_p = 10 \mu\text{SEC}$        $f_p = 10 \text{ KHZ}$   
 $P_{AV} = 2.3 \text{ KW}$      $P = 100 \text{ TOHR}$      $P_p = 150 \text{ W}$   
 $R = 0.95$

Figure A7. Typical laser output data with flowing gas for 3:0:1 mix. (Note: All photos 2  $\mu\text{sec/div}$  time scale.)

pulse was obtained with the 3:0:1 mix which also had the shortest decay tail as would be expected due to the absence of  $N_2$  in the mix. In the mixes containing  $N_2$  it is readily observed that a large fraction of the output energy occurs in the decay tail (50 percent). In general, the gas mixes with and without  $N_2$  had comparable power spike pulsewidths (~140 to 170 nsec). This pulsewidth was not recorded for every parametric data point but in general the pulsewidths just mentioned were typical for all the data listed in Table A2.

The polarization of the laser output was also measured. For both cw and pulsed operation, the laser output was self-polarized such that the electric field of the laser output was parallel to the electrode surfaces. This is an important result. No Brewster windows are needed internal to the resonator and thus optical losses are minimized when polarized output is desired.

It is again important to note that the output power results would have been significantly improved had internal optics been employed. The external resonator with internal AR windows introduces significant loss both due to the window losses and the bore coupling losses which are enhanced by the large index of refraction of the ZnSe windows.

#### SUMMARY OF THE FLOWING GAS EXPERIMENTS

The quality of the data obtained for the Phase 1 effort was excellent. The power electronics, diagnostic equipment, monitoring electronics, and detector electronics used in taking the data performed well with the exception of the pulsed rf supply and the contamination problem of the laser head. The latter problem was overcome by flowing the gas at a rapid rate and thus parametric variation of the gas flow was not performed since decreasing the flow rate from the maximum rates used in taking the data would have led to performance degradation due to the increased effects of the contamination problem. It should be noted that the contamination problem was solved after the completion of Phase 1 and no problem was observed in the sealed-off experiments of Phase 2.

DATE  
FILMED  
-8